Combined Quantum Mechanical and Molecular Mechanical Simulations of One- and Two-Electron Reduction Potentials of Flavin Cofactor in Water, Medium-Chain Acyl-CoA Dehydrogenase, and Cholesterol Oxidase†

Sudeep Bhattacharyya, Marian T. Stankovich,* Donald G. Truhlar,* and Jiali Gao*

Department of Chemistry and Supercomputing Institute, University of Minnesota, 207 Pleasant Street SE, Smith Hall, Minneapolis, Minnesota 55455-0431

Received: February 23, 2007; In Final Form: May 18, 2007

Flavin adenine dinucleotide (FAD) is a common cofactor in redox proteins, and its reduction potentials are controlled by the protein environment. This regulation is mainly responsible for the versatile catalytic functions of flavoenzymes. In this article, we report computations of the reduction potentials of FAD in medium-chain acyl-CoA dehydrogenase (MCAD) and cholesterol oxidase (CHOX). In addition, the reduction potentials of lumiflavin in aqueous solution have also been computed. Using molecular dynamics and free-energy perturbation techniques, we obtained the free-energy changes for two-electron/two-proton as well as one-electron/one-proton addition steps. We employed a combined quantum mechanical and molecular mechanical (QM/MM) potential, in which the flavin ring was represented by the self-consistent-charge density functional tight-binding (SCC-DFTB) method, while the rest of the enzyme−solvent system was treated by classical force fields. The computed two-electron/two-proton reduction potentials for lumiflavin and the two enzyme-bound FADs are in reasonable agreement with experimental data. The calculations also yielded the pK_a values for the one-electron reduced semiquinone ($FH^\bullet$) and the fully reduced hydroquinone (FH_2) forms. The pK_a of the FAD semiquinone in CHOX was found to be around 4, which is 4 units lower than that in the enzyme-free state and 2 units lower than that in MCAD; this supports the notion that oxidases have a greater ability than dehydrogenases to stabilize anionic semiquinones. In MCAD, the flavin ring interacts with four hydrophobic residues and has a significantly bent structure, even in the oxidized state. The present study shows that this bending of the flavin imparts a significant destabilization (∼5 kcal/mol) to the oxidized state. The reduction potential of lumiflavin was also computed using DFT (M06-L and B3LYP functionals with 6-31+G(d,p) basis set) with the SM6 continuum solvation model, and the results are in good agreement with results from explicit free-energy simulations, which supports the conclusion that the SCC-DFTB/MM computation is reasonably accurate for both $1e^-/1H^+$ and $2e^-/2H^+$ reduction processes. These results suggest that the first coupled electron−proton addition is stepwise for both the free and the two enzyme-bound flavins. In contrast, the second coupled electron−proton addition is also stepwise for the free flavin but is likely to be concerted when the flavin is bound to either the dehydrogenase or the oxidase enzyme.

1. Introduction

Enzyme cofactors play an essential role in many oxidation and reduction processes in biological systems. In many cases, the redox reactions are directly or indirectly coupled to proton-transfer events, and thus, the overall process can be described as a coupled electron−proton-transfer reaction.[1,2] Consequently, the reduction potentials typically depend on pH, which, in turn, influences the electron-transfer kinetics.[1,2] Flavoenzymes employ a flavin adenine dinucleotide (FAD) or a flavin mononucleotide (FMN, also called riboflavin 5′-phosphate) as the cofactor Figure 1, and the 7,8-dimethylisoalloxazine moiety of these cofactors acts as a redox mediator and shuttles between various redox states, formally by electron transfer between the flavin and the substrate.[3]

The reduction of FAD in aqueous solution involves two sequential one-electron- and one-proton-transfer reactions,[3,4] whereas FAD reduction in enzymes can occur via two possible routes, either through a one-electron reduction that produces a radical semiquinone or a full two-electron reduction that yields a hydroquinone.[3] Reactions catalyzed by flavoenzymes include oxidations, dehydrogenations, hydroxylations, and electron transfers. The versatility of this single cofactor arises from the effective tuning of the cofactor's reduction potential by the host protein. The bending of the tricyclic isoalloxazine ring (Figure 1) by the interacting enzyme environment is understood to be the key in such a modulation of the flavin's reduction potentials.[5] Indeed, the midpoint potentials, the pK_a values of the products, and the mechanism (stepwise vs concerted additions of electron (or hydride) and proton) of FAD are regulated by the specific interactions of the enzyme in the active site.[1,2,5−9] Computational studies of flavoenzymes can be valuable for understanding the underlying physical principles that control their reduction potentials and activities.

Reduction potentials of small organic molecules, metal ions, and electron-transfer proteins in condensed phases have been calculated successfully by combining electronic structure calculations (such as DFT) with a continuum solvation model[10−34]

† Part of the "DFTB Special Section".

* To whom correspondence should be addressed. E-mail: stankovi@chem.umn.edu (M.T.S); truhlar@umn.edu (D.G.T.); gao@chem.umn.edu (J.G.).

10.1021/jp071526+ CCC: $37.00
Published on Web 06/14/2007

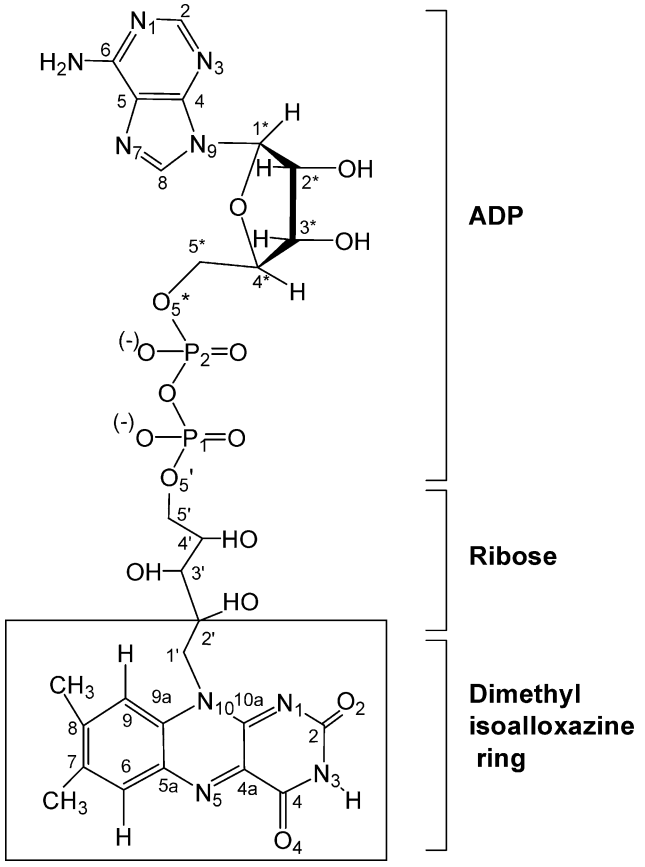

Figure 1. A molecular diagram of FAD showing various parts with atoms numbered. The 7,8-dimethyl isoalloxazine (flavin) ring was taken as the QM subsystem. In the thermodynamic integration simulation of the reduction step, C2′ was chosen as the boundary atom, and the QM/MM boundary is shown with a box. In the thermodynamic integration calculation of the pK_a, the link atom was placed between the C1′ and C2′ atoms.

or an explicit solvent and enzyme.[34−43] In the present study, we employ both approaches to determine flavin reduction potentials. Our main focus is the reduction potential of FAD in medium-chain acyl-CoA dehydrogenase (MCAD), which catalyzes the α,β-dehydrogenation reaction of medium-chain (C8-C14) acyl-CoA molecules in the first step of the β-oxidation pathway. MCAD has been extensively studied, and the reduction potentials for both one-electron/one-proton and two-electron/two-proton processes are available experimentally. Recently, the catalytic mechanisms of the α,β-dehydrogenation reaction of the short-chain (SCAD)[44] and the medium-chain (MCAD)[45] enzymes have been investigated in these laboratories using a combined QM/MM potential based on the Austin Model 1[46] (AM1) Hamiltonian for the active site and the CHARMM22 (Chemistry at Harvard Macromolecular Mechanics) force field[47] (CHARMM) for the enzyme. In both of these enzymes, we found that the α,β-dehydrogenation reaction is a stepwise process involving an initial α-proton abstraction by an active site base (Glu367 for SCAD and Glu376 for MCAD) followed by a hydride transfer from the β-carbon of the substrate to FAD.[45] Thus, the catalytic process in these enzymes can be thought of as a combination of two quasi-independent processes, and the factors influencing the flavin reduction can be studied separately from the substrate deprotonation, although we note that the present study is limited to the half-reduction potential rather than the hydride transfer between the substrate and FAD.

To determine the reduction potentials of the FAD cofactor, we have chosen the self-consistent-charge density functional tight-binding[48−50] (SCC-DFTB) method that has been parametrized against DFT results (in particular, B3LYP) for model systems. Rather than reparameterizing the AM1 model, we took advantage of the findings of a previous study, showing that the SCC-DFTB method can yield excellent results for the single-electron addition process of FAD in cholesterol oxidase (CHOX).[38,40]

To gain further insight into the role of the enzyme environment, we also studied lumiflavin (LF) as a model for FAD in aqueous solution. LF has the complete flavin moiety, but the 10′-ribose substituent of FAD is replaced by a methyl group. In particular, the free-energy changes are computed for electron and proton reactions of lumiflavin in the gas phase and in aqueous solutions and for FAD bound to MCAD. To check the present computational procedure, we also determined the one-electron reduction potential of FAD in the active site of cholesterol oxidase (CHOX) for comparison with a previous study.[38,40] From these calculations, we obtained both standard reduction potentials and pK_a values for the FAD semiquinone and hydroquinone in the enzymes.

In section 2, we describe the computational methods, which include free-energy calculations using both implicit and explicit treatment of the solvent. In the implicit solvent calculations, we employed a combination of M06-L and B3LYP density functional methods and an implicit solvent model, Solvation Model 6 (SM6), to compute the free-energy changes of the lumiflavin electron and proton addition reactions in aqueous solution. The free-energy calculations for these electron- and proton-transfer steps of lumiflavin were then repeated with SCC-DFTB both in the gas phase and in aqueous solution, in the latter case treating the solvent explicitly using combined QM/MM free-energy simulations. The calculations with explicit solvent were then extended to the enzyme systems, in which the flavin moiety of the FAD was treated by the SCC-DFTB method and the solvent modeled by CHARMM. In section 3, in addition to these computational results of both enzyme-bound FAD and unbound lumiflavin in water, we also discuss the effects of the enzyme environment on the standard reduction potential of the cofactor. Section 4 contains concluding remarks.

2. Methods and Computational Details

2.1. Electronic Structure Calculations. The structure and energy of lumiflavin have been determined in the gas phase by carrying out density functional theory (DFT) calculations with the M06-L[51] and Becke's 3-parameter Lee−Yang−Parr (B3LYP) density functionals[52−54] with the 6-31+G(d,p) basis set[55] and with the semiempirical AM1[46] and SCC-DFTB[48−50] methods. The SCC-DFTB model, like the earlier iterative extended Hückel approximation (IEHT),[56] incorporates a self-consistent-field treatment of electron−electron interactions into tight-binding[57] theory, and the electronic polarization is approximated by first-order perturbation in terms of atom-centered point charges obtained by Mulliken population analysis.[50,58] Extended Hückel theory has provided major insights into the understanding of chemical reactivity of organic and organometallic compounds; the key difference of the SCC-DFTB model from the iterative extended Hückel is that SCC-DFTB has recently been parametrized[48−50,59] to fit properties from B3LYP calculations, providing more quantitative results than those of IEHT.

2.2. Implicit Solvent. The implicit solvent calculations were carried out at 298 K with Solvation Model 6,[60] using the thermodynamic cycle of Scheme 1[33] for electron addition and Scheme 2[61] for proton addition. In these schemes, ΔG^o is the standard free energy of reaction either in the gas phase (*g*) or

SCHEME 1

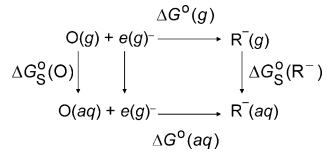

SCHEME 2

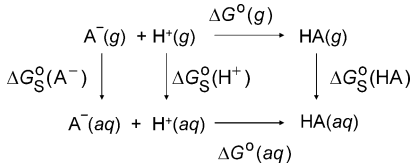

in aqueous solution (*aq*), and ΔG_S^o is the standard free energy of solvation. We used a standard state of a 1 atm ideal gas for gaseous species and a 1 M ideal solution for solutes. In calculating the solvation free energies, we used gas-phase M06-L or B3LYP geometries. In calculating gas-phase vibrational−rotational free energies at 298 K, we used the harmonic oscillator−rigid rotor approximation with unscaled B3LYP frequencies and moments of inertia. The electronic free energy was approximated as $-RT \ln d$, where R is the gas constant, T is the temperature, and d is the electronic degeneracy of the ground state (1 for singlet, 2 for doublets). The contribution of the electron to the standard-state free energy at 298 K is less than 0.02 kcal/mol[62] (1 meV) and was neglected. The calculations were carried out with the Gaussian03[63] and MN-GSM[64] computer programs.

2.3. Standard Reduction Potentials. Standard reduction potentials are usually expressed relative to the standard reduction potential of the normal hydrogen electrode,[65] E_H°, which is 4.28 V.[66] Therefore, the standard reduction potential of any of the reduction reactions considered in the article is

$$E^o = -\frac{\Delta G^\circ(aq)}{nF} - E_H^\circ \qquad (1)$$

where n is the number of electrons on the left side of the reaction and F is the Faraday constant, which equals 23.06 kcal mol^{-1} V^{-1}.

In aqueous solution, the first reduction of FAD is followed by protonation of the N5 atom; this produces neutral semiquinone (FH$^\bullet$, where F is shorthand for flavin, in this case FAD).[5,7] The neutral semiquinone is not very stable and rapidly undergoes the second reduction, yielding the fully reduced hydroquinone (FH_2). These reduction potentials are strongly pH dependent,[7] and if, at a certain pH, the reduction potentials of the oxidized → semiquinone and semiquinone → hydroquinone steps are denoted by $E_{ox,sq}$ and $E_{sq,rd}$, then the midpoint potential, E_m, can be defined[5,7] as an average of the two reduction potentials, that is

$$E_m = \frac{1}{2}(E_{ox,sq} + E_{sq,rd}) \qquad (2)$$

That the electron and proton addition steps are coupled is evident from the significant variations of the observed reduction potential values upon pH changes, and these effects are very well documented for flavin mononucleotide and riboflavin in aqueous solution[67] as well as FAD-bound MCAD.[67,68]

2.4. Stochastic Boundary Setup. Stochastic boundary molecular dynamics[69] were used in which either the model compound LF was immersed in the center of the solvent or the FAD cofactor was embedded in the enzyme active site. Each system was partitioned into three zones, the reaction zone (<24 Å), the buffer zone (24−30 Å), and the reservoir zone (>30 Å). The reaction zone atoms were completely free and were treated with Newtonian mechanics. The buffer zone atoms were treated by the Langevin equation of motion, with a friction coefficient and a random force imposed on non-hydrogen atoms. From the outer-Langevin boundary toward the inner zone, these friction coefficients as well as the random forces were gradually scaled down and set to zero at the reaction region boundary. The reservoir zone acted like a static force field, providing electrostatic interactions between the atoms in the reservoir region and atoms in the inner region. In addition, to contain the reaction zone, a deformable boundary potential[70] corresponding to a 30 Å solvent sphere was applied to all solvent atoms in the system.

The procedure for setting up the enzyme simulations is the same as that described in our studies[44,45] on acyl-CoA dehydrogenase catalysis. The protein coordinates of MCAD (PDB code 3MDD)[71] and CHOX (PDB code 1B4V)[72] were obtained from the protein databank.[73] The tetrameric MCAD was used in the present study since it has been well established for this group of enzymes. For CHOX, the coordinates represent a monomer, which was used in all simulations. All crystal water molecules were retained, and hydrogen atoms were added by using the HBUILD module of CHARMM (C32a1).[74] The setup for the enzyme-bound flavin was maintained identical to the one used for simulating the catalytic reaction of this enzyme.[45] All ionic amino acid residues were modeled in a protonation state corresponding to pH 7. Therefore, histidines were treated as neutral residues, and the position of the titratable proton was judged by inspecting hydrogen bonding interactions with the Nϵ or Nδ atoms of each imidazole moiety.

For the tetrameric MCAD, atoms of subunits C and D, which fall outside of a 45 Å radius from a chosen geometric center, defined as the average position of the flavin ring atoms, were deleted. The overall charge of the oxidized form of the solvated protein−cofactor complex was neutralized by adding counterions. Flavin is neutral in the fully oxidized state, and thus, the sum of the charges on the quantum mechanically treated atoms (the flavin moiety) and the molecular mechanically treated atoms (rest of the system) is equal to zero. For either electron or proton additions, the change in the charge state occurs only on the quantum mechanically treated atoms (see section 2.5), and the net charge of the molecular mechanically treated region remains the same (i.e., 0) through all simulations. To neutralize the molecular mechanically treated region, in the case of MCAD, a single chloride ion was added, whereas for CHOX, two calcium and one chloride ions were included. These ions were located within 30 Å of the geometric center (defined above). It is, however, significant to note that although the sum of the charges of the molecular mechanically treated region was unchanged in all simulations, the total (quantum mechanical plus molecular mechanical) charges in various spherical regions surrounding the redox active center, in the structures of the solvated protein−cofactor complex generated above, did undergo changes during electron- and proton-transfer processes. As described in the following section, these charges must be accounted for in order to accurately determine the solvation free energies of various redox states.

2.5. Born Corrections. Whereas the implicit solvent calculations include the full polarization effect of the solvent, the explicit-environment calculations involve static solvent in the reservoir zone. Therefore, these calculations require a correction

for polarization effects due to the region that is more than 30 Å from the reaction center. This correction was made using the Born formula[75,76] for a 30 Å cutoff for the lumiflavin. If the dielectric constant is D in the region beyond 30 Å, the Born approximation for the additional free-energy contribution is

$$\Delta G_{\text{Born}} = -\frac{q^2}{2R_1}\left[1 - \frac{1}{D}\right] \tag{3}$$

where q is the charge within the sphere of radius R_1 (which is 30 Å), and D is the solvent dielectric constant (approximated for the aqueous solution as 78 at 298 K).

Unlike solvated lumiflavin in the aqueous simulations, the reservoir zones (>30 Å) in the two protein−cofactor complexes were not pure water but rather contained some additional protein atoms. It is not clear what dielectric constant to use in the regions of 30−45 Å and 45−65 Å since they contain both protein and water. Since, for MCAD, the 30−45 Å and 45−65 Å shells contain about 50 and 10% protein atoms, respectively, we used a dielectric constant of 5 for the 30−45 Å shell and 30 for the 45−65 Å shell. The unbalanced charges for each of the 30, 45, and 65 Å spherical regions were calculated by summing the signed charges on all charged residues and counterions and the charged diphospho- moiety of the FAD in the respective shells. If the oxidized solvated enzyme−cofactor complex is designated by F, then the total unbalanced charges computed in this way for F in MCAD are −5 for the 30 Å sphere, +1 for the 45 Å sphere, and 0 for the 65 Å sphere (see Supporting Information Tables S1−S4). The Born solvation free energy is calculated as

$$\Delta G_{\text{Born}} = -\frac{q_1^2}{2R_1}\left(\frac{D_1 - 1}{D_1}\right) + \frac{q_1^2}{2R_2}\left(\frac{D_1 - 1}{D_1}\right) - \frac{q_2^2}{2R_2}\left(\frac{D_2 - 1}{D_2}\right) + \frac{q_2^2}{2R_3}\left(\frac{D_2 - 1}{D_2}\right) - \frac{q_3^2}{2R_3}\left(\frac{D_3 - 1}{D_3}\right) \tag{4a}$$

where, for F, $q_1 = -5$, $R_1 = 30$ Å, $D_1 = 5$, $q_2 = +1$, $R_2 = 45$ Å, $D_2 = 30$, $q_3 = 0$, $R_3 = 65$ Å, and $D_3 = 78$. In order to calculate ΔG_{Born} for each of the electron- and proton-transferred products, in eq 4a, only q_1, q_2, and q_3 need to be changed. For each electron and proton addition, the charge decreases and increases, respectively, by unity. Thus, for the anionic semiquinone ($F^{-\bullet}$) and hydroquinone (FH^-), $q_1 = -6$, $q_2 = 0$, and $q_3 = -1$; for the neutral semiquinone ($FH^\bullet$) and hydroquinone (FH_2), $q_1 = -5$, $q_2 = +1$, and $q_3 = 0$; and for the diionic hydroquinone (F^{2-}), $q_1 = -7$, $q_2 = -1$, and $q_3 = -2$.

In the CHOX case, there is about 10% protein in the 30−45 Å shell, which carries a charge of −3 (see Supporting Information Tables S5−S7) in the oxidized state of the bound cofactor. We used a dielectric constant of 30 for this region. Then, the solvation free energies for the solvated CHOX−FAD complex were computed by

$$\Delta G_{\text{Born}} = -\frac{q_1^2}{2R_1}\left(\frac{D_1 - 1}{D_1}\right) + \frac{q_1^2}{2R_2}\left(\frac{D_1 - 1}{D_1}\right) - \frac{q_2^2}{2R_2}\left(\frac{D_2 - 1}{D_2}\right) \tag{4b}$$

where, for the oxidized solvated protein−cofactor complex, designated by F, $q_1 = -3$, $R_1 = 30$ Å, $D_1 = 30$, $q_2 = 0$, $R_2 = 45$ Å, and $D_2 = 78$. Similar to the MCAD−FAD case, for the monoionic semiquinone ($F^{-\bullet}$) and hydroquinone, $q_1 = -4$ and $q_2 = -1$; for the neutral semiquinone ($FH^\bullet$) and hydroquinone (FH_2), $q_1 = -3$ and $q_2 = 0$; for the diionic hydroquinone (F^{2-}), $q_1 = -5$ and $q_2 = -2$. Then, for any reaction that involves a change in the charge state of the quantum mechanically treated region (the flavin ring atoms, as described in section 2.4), the contribution of solvation free energy was calculated by

$$\Delta\Delta G_{\text{Born}} = \Delta G_{\text{Born}}(\text{P}) - \Delta G_{\text{Born}}(\text{R}) \tag{5}$$

where P denotes product, and R denotes reactant.

2.6. Molecular Dynamics Simulations. For enzyme-bound complexes, the energy of the active site with the cofactor molecule was first minimized prior to the MD simulations. Initially, the minimization was carried out only with respect to the coordinates of the QM atoms; this was done using 40 steps of the adopted basis Newton−Raphson minimization algorithm. Next, 100 cycles of such minimization were carried out by fixing the QM atoms and all of the atoms beyond 30 Å of the active site center. The enzyme−cofactor complex was further solvated with a water sphere of radius 30 Å following previously established procedures.[45,69] Water molecules within 2.5 Å of any non-hydrogen atoms were deleted. To relax unfavorable contacts, dynamics simulations were performed for 5 ps. This was repeated to fill in any cavity generated during dynamic relaxation, and the system was further equilibrated by 5 ps of MD simulation.

Molecular dynamics (MD) simulations of the aqueous lumiflavin and the FAD-bound enzyme systems were carried out with the program CHARMM (c32a1).[74] The tricyclic isoalloxazine ring atoms were treated with SCC-DFTB (Figure 1), and the rest of the atoms of the cofactor and protein were treated with the CHARMM22[77,78] all-atom force field. Solvent water molecules were treated by the three-point-charge TIP3P model.[79] The nonbonded interactions were truncated using a switching function between 12 and 14 Å, and the dielectric constant was kept at unity. The SHAKE algorithm[80] was used to constrain the bond lengths and bond angles of the hydrogen atoms. A time step of 1 fs was used in the leapfrog Verlet algorithm for integration.[81,82]

In all simulations, the QM/MM boundary consists of a single atom, C2′. This boundary atom was treated either with the generalized hybrid orbital (GHO) method[83,84] (for electron addition) or by a hydrogen-link atom method[85] (for proton addition).

2.7. Thermodynamic Integration. The free-energy changes for electron and proton dissociations were calculated by the Kirkwood thermodynamic integration scheme.[38,40,86−92] If we define the initial state (electron or proton absent) as $\lambda = 0$ and the final state (electron or proton bound) as $\lambda = 1$, the free-energy difference between the two states is given as follows

$$\Delta G(0 \rightarrow 1) = \int_0^1 d\lambda \left\langle \frac{\partial U(\lambda)}{\partial \lambda} \right\rangle_\lambda \tag{6}$$

where the average $\langle \cdots \rangle_\lambda$ is over the potential $U(\lambda)$. A convenient choice for the potential $U(\lambda)$ that couples the system from the initial to the final state is given by

$$U(\lambda) = (1 - \lambda)U_i + \lambda U_f \tag{7}$$

where U_i and U_f are the potential energy functions of the initial and final state, respectively. Thus, eq 6 becomes the integration of the average in the difference between the two potentials[39] as the coupling parameter varies from 0 to 1

$$\Delta G(0 \rightarrow 1) = \int_0^1 d\lambda \langle U_f - U_i \rangle_\lambda \tag{8}$$

It is important to emphasize that the potential energies, U_i and U_f, in eq 8 are evaluated in the ensemble corresponding to $U(\lambda)$. In practice, eq 8 is integrated numerically by carrying out a series of simulations at fixed values of λ. An interesting feature of eq 8 is that energy components are additive and can be separated to probe specific contributions to the overall free-energy change, although such computations only provide qualitative insight since the numerical results are path dependent.[89]

Specifically, in the present study, we use a combined QM/MM potential to describe the cofactor−enzyme−solvent system, and the total potential energy for state A is given as follows

$$U_A = \langle \Psi(A)|H^{\circ}_{qm}(A) + H_{qm/mm}(A)|\Psi(A)\rangle + U_{mm} \quad (9)$$

where $H^{\circ}_{qm}(A)$ is the Hamiltonian of the QM subsystem (e.g., flavin) in the gas phase, U_{mm} is the classical (MM) potential energy of the remainder of the system, $H_{qm/mm}(A)$ is the QM/MM interaction Hamiltonian between the two regions, and $\Psi(A)$ is the molecular wave function of the QM subsystem optimized for $H^{\circ}_{qm}(A) + H_{qm/mm}(A)$. Although it is straightforward to substitute the potential energies in eq 9 for the corresponding expressions given by eq 8, it is more convenient to rewrite eq 9 as follows[93]

$$U_A = E^{\circ}_g(A) + \Delta U_{qm/mm}(A) + U_{mm} \quad (10)$$

where $E^{\circ}_g(A)$ is the intrinsic (gas phase) energy of an isolated QM subsystem, $E^{\circ}_g(A) = \langle \Psi^o(A)|H^{\circ}_{qm}(A)|\Psi^o(A)\rangle$, and $\Delta U_{qm/mm}(A)$ is the interaction energy between the QM and MM regions defined as

$$\Delta U_{qm/mm} = \langle \Psi(A)|H^{\circ}_{qm}(A) + H_{qm/mm}(A)|\Psi(A)\rangle - E^{\circ}_g(A) \quad (11)$$

With the energy terms of eq 11, we obtain the following equation for QM/MM free-energy simulations

$$\Delta G(0 \rightarrow 1) = \int_0^1 d\lambda \langle \Delta E^{\circ}_g(i \rightarrow f) + \Delta\Delta U_{qm/mm}(i \rightarrow f)\rangle_\lambda \quad (12)$$

The notation $\Delta E^{\circ}_g(i \rightarrow f)$ specifies the gas-phase energy difference between the initial and final states, and $\Delta\Delta U_{qm/mm}(i \rightarrow f)$ is the difference in interaction energies between the initial and final states, both at the instantaneous coordinates of each MD simulation step. The separation of the gas-phase energy term in eq 12 allows high-level energy results to be conveniently used to correct the intrinsic errors in the SCC-DFTB method (see below). The same approach has been described by Cui and co-workers.[40,92]

In the dual-topology, single-coordinate[40,83,92] calculations for various electron and proton addition reactions, which are explained in sections 2.8 and 2.9 below, we made a further approximation, namely, that the van der Waals interactions between the QM and MM regions are the same for the initial and final state. This is partly justified by our previous study[45] of the catalytic reactions in MCAD, where it was found that the coordinates of flavin in the MCAD active site did not undergo any major change before and after the catalytic hydride transfer. There was no conformational change in the immediate surroundings of the flavin either, as was demonstrated by the evolution of hydrogen-bonding distances along the whole reaction path.[45]

2.8. Free Energies of Electron Addition. Following the work of Cui and co-workers, we used a dual-topology, single-coordinate approach for the electron-transfer reactions. In this approach, the initial and final states share the same atomic coordinates. Consider the case of electron addition

SCHEME 3

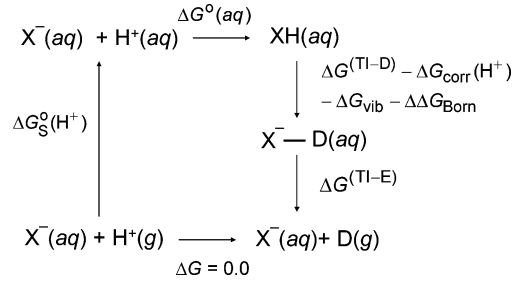

$$O + e^- \rightarrow R \quad (A)$$

where R shares the same atomic coordinates as O except that it has one more electron. Note that, depending on the reaction, either O or R may be charged (positive or negative) or be neutral. For each electron addition processes, 11 values (for MCAD−FAD) and 6 values (for LF and CHOX−FAD) of λ were used, evenly spaced from 0 to 1, with a combined ∼1.5 ns MD simulation for MCAD−FAD and an ∼1 ns MD simulation for LF and CHOX−FAD. Equation 12 was integrated numerically. The overall free-energy change is given by

$$\Delta G^{\circ}(aq) = \Delta G^{(TI-A)} + \Delta\Delta G^{(A)}_{Born} + \Delta G_{quantal} + HLC \quad (13)$$

where $\Delta G^{(TI-A)}$ is calculated by eq 12 for reaction A, $\Delta\Delta G_{Born}$ (see section 2.5) is a correction for truncating the dynamical region (reaction zone plus buffer zone) at 30 Å,[75,76] and $\Delta G_{quantal}$ is the correction for quantum mechanical effects given by

$$\Delta G_{quantal} \cong \Delta G_{elec} + \Delta G_{vib} \quad (14)$$

where

$$\Delta G_{elec} = -RT\ln\frac{d(P)}{d(R)} \quad (15)$$

where d is the electronic degeneracy, P denotes product, R denotes reactant, R is the universal gas constant, and T is the temperature. We have used the B3LYP results for the gas-phase free-energy difference in the $\Delta E^{\circ}_g(i \rightarrow f)$ term to correct errors in the SCC-DFTB method in eq 12, giving rise to the high-level correction (HLC) term in eq 13, which amounts to a difference of −7 and −4.8 kcal/mol from the SCC-DFTB treatment of the QM subsystem, as determined for the reactions $LF \rightarrow LF^{-\bullet}$ and $LF^{-\bullet} \rightarrow LF^{2-}$, respectively (vide infra).

2.9. Free Energies of Proton Addition. Next, consider a proton addition reaction. We will directly simulate only reactions where a proton is added to a negatively charged species as in

$$X^-(aq) + H^+(aq) \rightarrow XH(aq) \quad (B)$$

(see Scheme 3). (Note that free energies for reactions like

$$Y(aq) + e^- + H^+(aq) \rightarrow YH(aq) \quad (C)$$

will later be obtained by adding free-energy changes for reactions of types A and B, with O = Y and R = X^-).

As illustrated in Scheme 3, in order to calculate the free-energy change for reaction B, the free-energy changes of the following four steps are needed. In the first two steps, two

separate thermodynamic integrations are carried out,[92] one for

$$X^-H(aq) \rightarrow X^- - D(aq) \qquad (D)$$

and one for

$$X^- - D(aq) \rightarrow X^-(aq) + D(g) \qquad (E)$$

where D is a dummy atom, which has no QM interactions with X^- but possesses van der Waals interactions. The free-energy changes of these two steps are called $\Delta G^{(TI-D)}$and $\Delta G^{(TI-E)}$, respectively, and are calculated by eq 12. However, in order to calculate the free-energy change of the reaction in eq D, one has to add three correcting terms. The first correction, $\Delta G_{corr}(H^+)$, is to account for the incorrect self-energy treatment of the proton treated by SCC-DFTB[58] and is equal to −141.8 kcal/mol. The two other corrections are due to the vibration (ΔG_{vib}) and the Born correction ($\Delta\Delta G_{Born}$), analogous to the electron addition method described earlier.

The free-energy changes for the remaining two steps are known. The free-energy change for converting the gas-phase dummy atom into a gas-phase proton

$$X^-(aq) + D(g) \rightarrow X^-(aq) + H^+(g) \qquad (F)$$

can be taken as 0 kcal/mol, and the free-energy change for the reaction

$$X^-(aq) + H^+(g) \rightarrow X^-(aq) + H^+(aq) \qquad (G)$$

is equal to the standard free-energy of solvation of a proton, $\Delta G_S^\circ(H^+)$, which is equal to −264.0 kcal/mol[66,94,95] at the standard state (1 atm for the gaseous state and 1 mol/L for the solution state).

Then, by Scheme 3, the standard-state free-energy change for reactions of type B is given by

$$\Delta G^\circ(aq) = -\Delta G^{(TI-D)} + \Delta G_{corr}(H^+) + \Delta\Delta G^{(B)}_{Born} + \Delta G_{vib} - \Delta G^{(TI-E)} - \Delta G_S^\circ(H^+) + HLC \qquad (16)$$

where the HLCs are +5.8 kcal/mol for $LF^{2-} + H^+ \rightarrow LFH^-$ and −0.3 kcal/mol for $LFH^- + H^+ \rightarrow LFH_2$.

In carrying out the integral over λ from 0 to 1 (eq 12 for reaction D) in the current studies, we experienced end-point problems for $\lambda = 1$ in the pK_a calculation steps. Since the free-energy derivatives were found to be linear with λ, these end-point values at $\lambda = 1$ were obtained from extrapolation.

The dummy atom has the same mass and van der Waals parameters as a proton but has no charge. Thus, at the end state of reaction D, the dummy atom does not have any quantum mechanical electrostatic interactions with A^-, although it continues to interact with A^- through classical van der Waals interactions. As elaborated in the Li et al. article,[92] to accomplish complete deprotonation, one needs to transfer the dummy atom to the gas phase by removing the classical van der Waals and bonded interactions between the dummy atom and the rest of the system. This is accomplished in step E, for which the free-energy change, $\Delta G^{(TI-E)}$, has two components, $\Delta G^{(E)}_{vdw,D}$ and $\Delta G^{(E)}_{bonded,D}$, representing the free-energy changes for reaction E due to removal of the van der Waals and bonded interactions, respectively, of the dummy atom D with the rest. The removal of the van der Waals interaction is done by switching off the van der Waals parameters in a thermodynamic integration. In some previous calculations[92,96] employing this method, the calculated $\Delta G^{(E)}_{vdw,D}$ values were found to be insignificant.

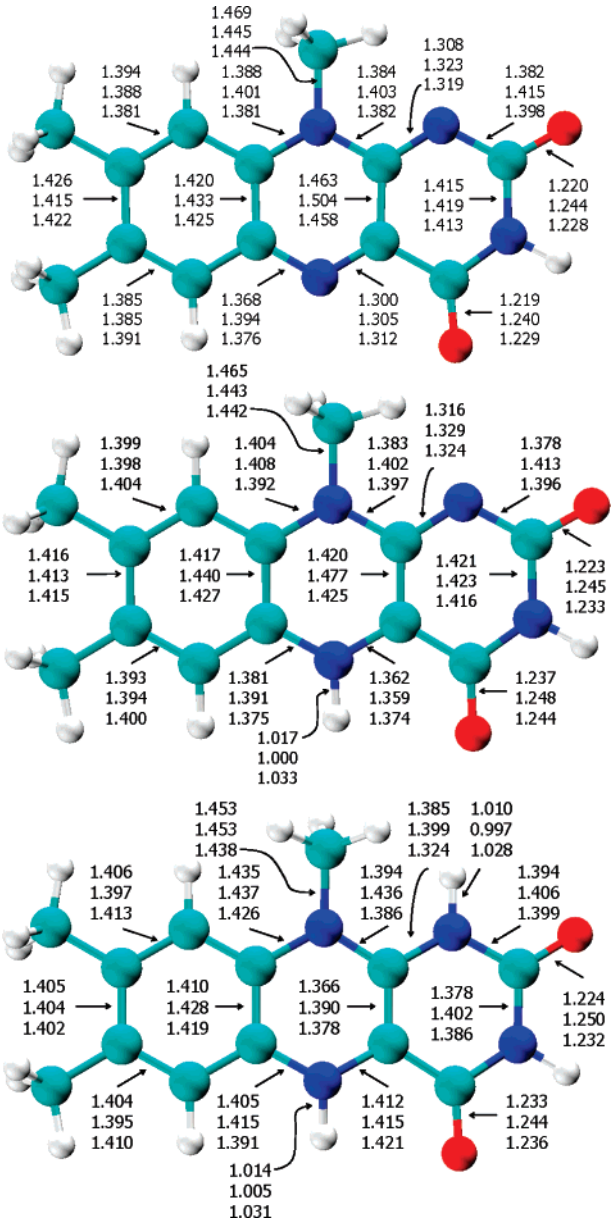

Figure 2. Comparison of the gas-phase bond lengths (Å) for the optimized structures of the oxidized lumiflavin (top panel), its semiquinone (middle panel), and the fully reduced hydroquinone (bottom panel). In each panel, the bond lengths are from B3LYP (top value), AM1 (middle value), and SCC-DFTB (bottom value). The C, H, N, and O atoms are shown in cyan, white, blue, and red, respectively.

Thus, in the present calculation, $\Delta G^{(E)}_{vdw,D}$ was ignored, and $\Delta G^{(TI-E)}$ was set equal to $\Delta G^{(E)}_{bonded,D}$.

The bonded contributions $\Delta G^{(E)}_{bonded,D}$ were estimated in terms of local properties by the method of Herschbach et al.[97] This yielded[92,97,98]

$$\Delta G^{(E)}_{bonded,D} = -RT\ln\frac{V_0\Lambda_D^{-1}}{(r^2/\sin\Psi)(2\pi k_B T)/K_\theta} + \frac{5}{2}RT \qquad (17)$$

where k_B is Boltzmann's constant, V_0 and Λ_D are the molar volume and thermal wavelength, respectively, of the dummy atom, r and Ψ represent the distance of the dummy atom to the flavin ring nitrogen atom (N5 or N1) and the angle between the two planes, D−N5(N1)−C7 and D−N5(N1)−C3, and K_θ

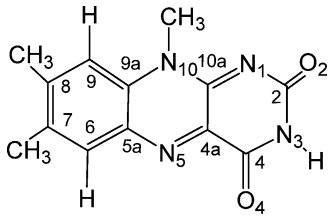

Figure 3. A molecular diagram of lumiflavin with atoms numbered.

is the bending force constants for the two bond angles, D-N5-(N1)-C7(C3) and D-N5(N1)-C3.

3. Results and Discussion

3.1. Lumiflavin in the Gas-Phase. Although recent applications of SCC-DFTB have been successful[96,99−103] to some problems, it is essential to validate it for the present kind of system. Here, we present SCC-DFTB results on the structures and the electron and proton affinities of a model FAD system, namely, lumiflavin (LF).

Figure 2 depicts the relevant bond lengths obtained using B3LYP, AM1, and SCC-DFTB for the three redox states, including the neutral LF, the $1e^-/1H^+$ reduced form LFH•, and the fully reduced form LFH_2. During $1e^-/1H^+$ reduction, a proton was added onto the N5 nitrogen (see Figure 3 for atom numbering), which increased the C4a−N5 bond lengths by 0.06 Å. Both AM1 and SCC-DFTB results are in agreement with the B3LYP values. Similarly, the C10a−N1 bond distance increased by 0.07 Å upon the second reduction and subsequent addition of the second proton to the N1 nitrogen ring. Again, both AM1 and SCC-DFTB models correctly reproduce this change. This shows that both SCC-DFTB and AM1 can adequately model the bond length variations during the reduction and protonation process.

A characteristic structural feature accompanying the flavin reduction is the formation of a butterfly-like configuration (Figure 4).[5] The extent of this structural bending in the fully reduced hydroquinone, which lacks aromaticity,[104] has been proposed to be critical for the catalytic efficiencies of flavoenzymes.[5] Thus, the midpoint potential E_m of FAD varies from −0.49 to +0.19 V in different flavoenzymes, largely responsible for the different reactivities of these enzymes.[6−8] For comparison, E_m is −0.22 V in water.[105] If the butterfly bend angle, θ_B, is defined as the angle between the planes of the pyrimidine and benzene six-membered rings, the computed structures give the bend angle as 155° in B3LYP, 157° in AM1, and 167° in SCC-DFTB. The SCC-DFTB model overestimates θ_B by 12° in comparison with the DFT value, whereas AM1 is almost perfect with respect to the B3LYP bending angle.

TABLE 1: Compared Gas-Phase Energies (kcal/mol) of Reaction of Electron and Proton Addition Steps of Lumiflavin[a], Calculated with M06-L and B3LYP (in Parenthesis)

reaction	M06-L (B3LYP)	SCC-DFTB[b]	AM1[c]
$LF + e^- \rightarrow LF^-$	−41 (−44)	−37	−64
$LF^- + H^+ \rightarrow LFH$	−335 (−334)	−334	−314
$LF + e^- + H^+ \rightarrow LFH$	−376 (−378)	−371	−378
$LF^- + e^- \rightarrow LF^{2-}$	57 (53)	58	48
$LF^{2-} + H^+ \rightarrow LFH^-$	−438 (−437)	−442	−420
$LF + 2e^- + H^+ \rightarrow LFH^-$	−422 (−428)	−421	−435
$LFH + e^- \rightarrow LFH^-$	−45 (−49)	−50	−57
$LFH^- + H^+ \rightarrow LFH_2$	−333 (−332)	−332	−320
$LF + 2e^- + 2H^+ \rightarrow LFH_2$	−755 (−760)	−753	−755

[a] The quantity tabulated is the Born−Oppenheimer energy difference of products from reactants. It includes electronic energy and nuclear repulsion but not vibrational or thermal effects. [b] As previously established,[58] a value of −141.8 kcal/mol was used as the reference for the proton to account for its self-interaction energy in DFTB calculations. [c] A previously established value of 365.7 kcal/mol was used as the standard heat of formation of a proton.[94]

The electron and proton affinities calculated by M06-L, B3LYP, AM1, and SCC-DFTB are given in Table 1. The calculated gas-phase energies with M06-L and B3LYP are within 5 kcal/mol. The AM1 model overestimates the first electron affinity (EA) of LF by 20 kcal/mol and underestimates the second EA by −5 kcal/mol. On the other hand, SCC-DFTB underestimates the EAs by −7 and −5 kcal/mol, respectively (Table 1). Note that the second EA of the model compound LF is positive. For the three proton addition reactions, the SCC-DFTB results are in better agreement with B3LYP results than those from AM1. The differences from the B3LYP results for the $LF^{-\bullet} \rightarrow LFH^\bullet$, $LF^{2-} \rightarrow LFH^-$, and $LFH^- \rightarrow LFH_2$ are 0, −5, and 0 kcal/mol, respectively, in SCC-DFTB calculations, and 20, 17, and 12 kcal/mol for AM1. For the overall $1e^-/1H^+$ ($LF \rightarrow LFH^\bullet$) and $2e^-/2H^+$ ($LF \rightarrow LFH_2$) processes, SCC-DFTB results are 7 and 6 kcal/mol less exothermic, while they are 0 and 5 kcal/mol less exothermic in AM1 calculations (Table 1) compared to the B3LYP results. Thus, there is a good error cancellation in the AM1 method. These enthalpy differences may be treated as intrinsic errors of the approximate quantum models and used as corrections to obtain the best estimate of reduction potentials. The SCC-DFTB model yields better agreement with the DFT results than the AM1 model for the electron and proton addition reactions of lumiflavin.

3.2. Lumiflavin in Aqueous Solution. The results for the aqueous standard free energies of reaction, that is, the bottom part of Schemes 1 and 2, were obtained from the thermodynamic cycles of the two schemes and are given in the $\Delta G°(aq)$ column

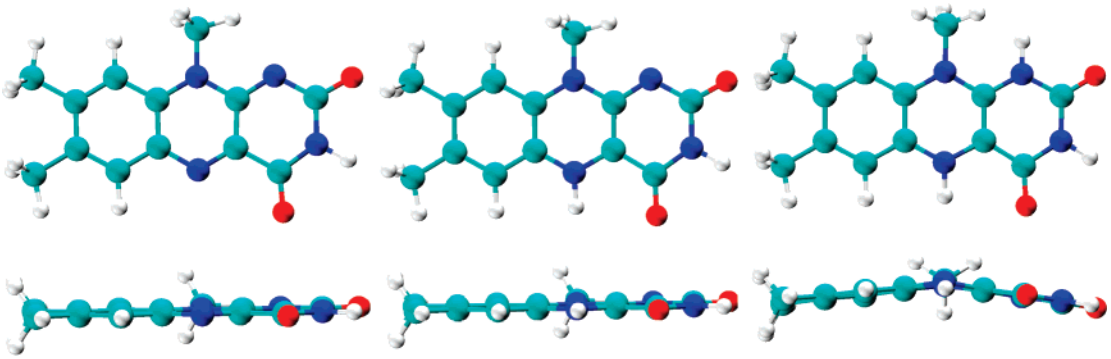

Figure 4. Structure and bending of the tricyclic isoalloxazine ring in lumiflavin. Displayed molecules from the left correspond to the neutral, semiquinone, and hydroquinone forms of lumiflavin. Top and bottom panel views are perpendicular and parallel to the isoalloxazine ring plane, respectively. Color codes are identical to those used in Figure 2.

TABLE 2: Standard Free Energies (kcal/mol) of Reactions for the Electron and Proton Additions to Lumiflavin in Water at 298 K, Calculated with Implicit Solvent with M06-L/SM6 and B3LYP/SM6 (in Parenthesis) and with Explicit Solvent Treatment with SCC-DFTB/CHARMM

	M06-L/SM6 (B3LYP/SM6)				SCC-DFTB/MM simulations
reactions	$\Delta G^o(g)$	$\Delta G_S^o(P)$	$\Delta G_S^o(R)$	$\Delta G^o(aq)$	$\Delta G^o(aq)$
$LF + e^- \rightarrow LF^{-\bullet}$	−43 (−47)	−63 (−67)	−22 (−23)	−84 (−91)	−93
$LF^{-\bullet} + H^+ \rightarrow LFH^\bullet$	−320 (−318)[a]	−22 (−24)	−327 (−331)[b]	−15 (−11)	−4
$LF + e^- + H^+ \rightarrow LFH^\bullet$	−363 (−365)	−22 (−24)	−286 (−287)	−99 (−102)	−97
$LFH^\bullet + e^- \rightarrow LFH^-$	−47 (−51)	−63 (−64)	−22 (−24)	−88 (−91)	−97
$LFH^- + H^+ \rightarrow LFH_2$	−316 (−317)[a]	−13 (−14)	−327 (−328)[b]	−2 (−3)	4
$LFH^\bullet + e^- + H^+ \rightarrow LFH_2$	−363 (−368)	−13 (−14)	−286 (−288)	−90 (−94)	−93
$LF + 2e^- + 2H^+ \rightarrow LFH_2$	−726 (−733)	−13 (−14)	−550 (−551)	−189 (−196)	−190

[a] The calculation includes a Gibb's free energy of H^+ of −6.28 kcal/mol.[117] [b] The solvation free energy of a proton, −264.0 kcal/mol in the standard state (1 atm for the gas phase and 1 mol/L for the solution state), is included.[66,94]

SCHEME 4

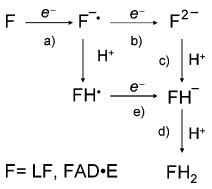

of Table 2. In addition, Table 2 also contains the comparative free-energy values, computed using the implicit and explicit solvent calculations. The overall $2e^-/2H^+$ free-energy changes in the implicit calculation for the reaction $LF + 2e^- + 2H^+ \rightarrow LFH_2$ are −189 and −196 kcal/mol when calculated by M06-L/SM6 and B3LYP/SM6, respectively (Table 2). The midpoint potential, E_m, of lumiflavin, computed using eq 1 with $n = 2$ and $E_H^\circ = 4.28$ V,[66] is therefore equal to −182 mV with M06-L and −30 mV with B3LYP. These calculated reduction potentials are 77 (with M06-L) and 229 mV (with B3LYP) less negative than the experimental result[106] of −259 mV.

In the explicit solvent calculation, various electron and proton addition steps (Scheme 4) were carried out with SCC-DFTB/MM. For these steps, the plots of the variations of the ensembled-averaged partial derivatives of the potential energy are shown in Figure 5. Judging from these plots of the ensemble-averaged $\langle U_f - U_i \rangle_\lambda$ with λ, it becomes evident that the free-energy derivative has a linear dependence on the net fractional charge of the redox center created by the coupling parameter λ. This is in conformity with the theory of a linear response[107] of the dielectric properties of an enzyme active site due to a change of the charge state at that site. In the explicit calculation, the $2e^-/2H^+$ free-energy change was found to be −190 kcal/mol (Table 2), which is very similar to the results of the implicit calculation. Using eq 1, the midpoint potential was calculated to be −160 mV and is within 100 mV of the experimental[106] value. Both implicit and explicit calculations showed that the N1 proton in the reduced hydroquinone is acidic. The standard free-energy change $\Delta G°(aq)$ for $FH^- + H^+ \rightarrow FH_2$ was computed as −2, −4, and 4 kcal/mol using M06-L/SM6, B3LYP/SM6, and SCC-DFTB/ CHARMM, respectively. The pK_a can be calculated from $\Delta G°(aq)$ using eq 18

$$pK_a = \frac{\Delta G°(aq)}{2.303RT} \tag{18}$$

The pK_a obtained for the N1 proton of lumiflavin hydroquinone using the three methods is 1.5 with M06-L/SM6, 3 with B3LYP/SM6, and −3 with SCC-DFTB/CHARMM.

3.3. Enzyme-Bound FAD. *3.3.1. Experimentally Observed Reduction Potentials.* Experimentally determined midpoint potential values for the overall $2e^-/2H^+$ reduction process of MCAD-bound FAD are available from the studies conducted by two independent groups. The two observed potential values are quite close; a value of −139 mV was reported by Guastafson et al.,[108] while Stankovich et al. obtained −136 mV[109] for the reaction $F + 2e^- + 2H^+ \rightarrow FH_2$, in both cases with respect to the standard reduction potential of the NHE, which is 4.28 V.[66] The overall free-energy change is therefore equal to −191 kcal/mol (eq 1). For the $1e^-/1H^+$ reduction (i.e., the $F + e^- + H^+ \rightarrow FH^\bullet$ reaction), only one group has reported observing an intermediate neutral semiquinone formation.[108] Although the amount of semiquinone formed during the two-electron/two-proton reduction process was small (~20% of all of the species present), they were able to estimate the first reduction potential ($E_{ox,sq}$) for MCAD−FAD as −155 mV at pH 7.1.[108] Taking the standard free-energy change for the reduction reaction at the NHE as −98.7 kcal/mol (−4.28 eV), this potential corresponds to standard free-energy change of −95 kcal/mol.

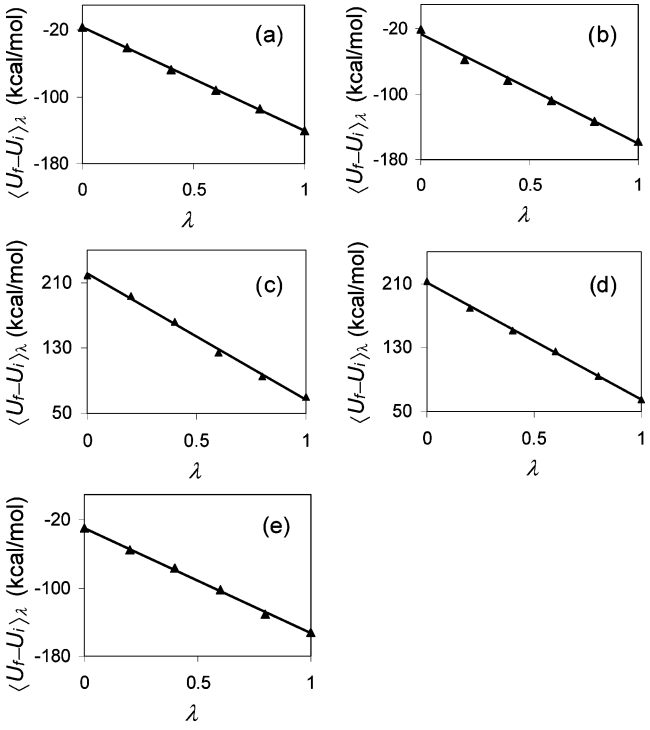

Figure 5. Ensemble-averaged partial derivatives of the potential energy versus the coupling parameter (λ) for lumiflavin. The various steps, as shown in Scheme 4, are (a) $LF \rightarrow LF^{-\bullet}$; (b) $LF^{-\bullet} \rightarrow LF^{2-}$; (c) $LF^{2-} \rightarrow LFH^-$; (d) $LFH^- \rightarrow LFH_2$; (e) $LFH^\bullet \rightarrow LFH^-$.

The reduction potential of cholesterol oxidase (CHOX) is also available from the literature.[110] The reductions of oxidases

(including CHOX) are distinctly different from those of dehydrogenases in the sense that the reduction in oxidases passes through a species $F^{-\bullet}$, the red anionic semiquinone,[6] as contrasted to the blue neutral semiquinone discussed in the previous paragraph. The reported E_m for the overall $2e^-/2H^+$ reduction is -278 mV,[110] which amounts to a free-energy change of -185 kcal/mol, with the standard free-energy change for the reduction reaction at the NHE taken as -98.7 kcal/mol. The $E_{ox,sq}$ is reported as -222 ± 14 mV,[110] which corresponds to a free-energy change of ca. -94 kcal/mol for the $F + e^- + H^+ \rightarrow FH^\bullet$ reaction.

3.3.2. Free-Energy Calculations. To obtain a $2e^-/2H^+$ reduction potential of MCAD−FAD and CHOX−FAD, analogous to the one already discussed for LF, the free-energy calculations for the two successive electron additions and two successive proton additions were carried out using thermodynamic integrations. Thus, representing the flavin ring of lumiflavin and the FAD-bound enzymes by a common name F (i.e., F = LF or FAD), the calculation gives free energies for the steps denoted by $F \rightarrow F^{-\bullet}$, $F^{-\bullet} \rightarrow F^{2-}$, $F^{2-} \rightarrow FH^-$, and $FH^- \rightarrow FH_2$ (Scheme 4). The first two steps consist of two sequential electron additions onto the neutral F, producing F^{2-}. A proton was added first to the N5 nitrogen of the F^{2-}, followed by a second proton addition on the N1 nitrogen of the FH^-. Since the free energy is independent of the path, the order of addition of the proton does not matter in this case, but it is relevant for the calculation of the $1e^-/1H^+$ potential, which is explained below. Free-energy changes for both proton additions were obtained by calculating the pK_a's for the respective protonated forms. Thus, to obtain a free-energy change in the $F^{2-} \rightarrow FH^-$ step, the pK_a of N5 nitrogen of the flavin ring was calculated, while for the $FH^- \rightarrow FH_2$ step, the free-energy change of the N1 deprotonation was computed.

To obtain the $1e^-/1H^+$ reduction potential, another thermodynamic integration was needed for the one-electron reduction of the $FH^\bullet \rightarrow FH^-$ step. The free-energy change for the $F \rightarrow FH^\bullet$ process was calculated from the thermodynamic cycle in Scheme 4

$$\Delta G^\circ_{F\rightarrow FH^\bullet} = \Delta G^\circ_{F\rightarrow F^{-\bullet}} + \Delta G^\circ_{F^{-\bullet}\rightarrow F^{2-}} + \Delta G^\circ_{F^{2-}\rightarrow FH^-} - \Delta G^\circ_{FH^\bullet\rightarrow FH^-} \quad (19)$$

The first two and the fourth terms in eq 19 correspond to electron addition processes, and the third one represents a proton addition. For the proton addition step, one faces an uncertainty: which nitrogen of the one-electron reduced FAD^- will bear the added proton, N5 or N1 of the isoalloxazine ring (Figure 1)? It is known that in flavoenzymes, the flavin N5 atom is the locus in the uptake/release of redox equivalents.[104] Furthermore, solution NMR studies of flavin mononucleotide indicate that the pK_a of N5 protons for fully reduced flavins is much higher ($\geq$20) than that of the N1 proton;[104,111] therefore, the proton on the semiquinone radical will most likely reside on N5. Therefore, in the $F^{2-} \rightarrow FH^-$ step, a proton was added onto the N5 atom of the isoalloxazine ring.

3.3.3. MCAD-Bound FAD. The variations of $\langle U_f - U_i \rangle_\lambda$ with λ for various steps shown in Scheme 4 are plotted in Figure 6. The free-energy estimates of various steps for the MCAD-bound FAD are given in Tables 3 and 4, and the reduction potentials and pK_a's are given in Table 5. Free-energy changes obtained from this study show that both electron-transfer steps occur with similar energetics. The computed free-energy changes are -81 and -76 kcal/mol for the first ($F \rightarrow F^{-\bullet}$) and the second ($F^{-\bullet} \rightarrow F^{2-}$) electron-transfer steps, respectively (Table 4). The calculated free-energy changes for the proton additions reactions

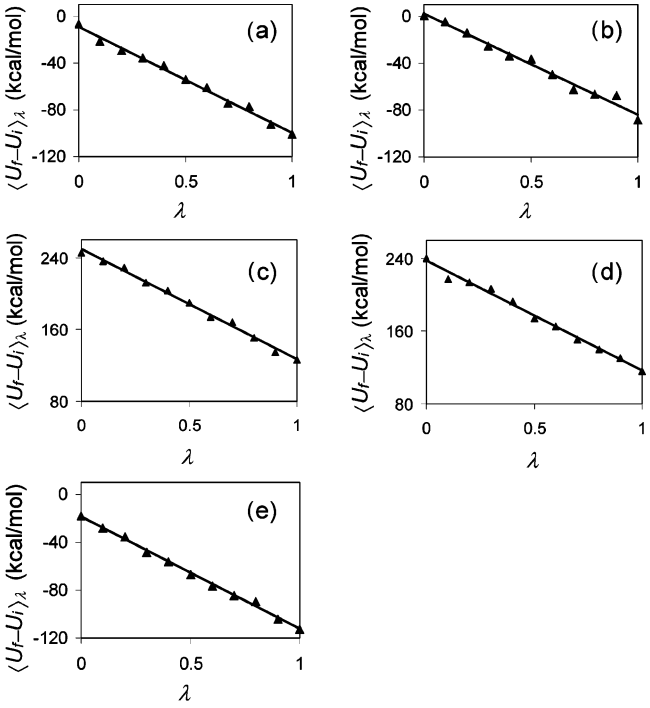

Figure 6. Ensemble-averaged partial derivatives of the potential energy versus the coupling parameter for various flavin reduction steps of MCAD−FAD. The steps are as shown in Scheme 4.

TABLE 3: Various Components of the Standard Free Energies of Reaction (kcal/mol) as Described in Eqs 13 and 16 (Sections 2.8 and 2.9) for Electron and Proton Addition Reactions of F at 298 K, Where F Is a Shorthand Notation for Flavin in Aqueous and Enzyme-Bound States

reaction	free-energy changes ΔG^o	
$F + e^- \rightarrow F^{-\bullet}$	$\Delta\Delta G_{Born}$	-5.5^a $(-17.7)^b$ $(-16.1)^c$
	ΔG_{vib}	-1.9
	HLC	-7.0
$F^{-\bullet} + e^- \rightarrow F^{2-}$	$\Delta\Delta G_{Born}$	-16.5^a $(-27.8)^b$ $(-27.0)^c$
	ΔG_{vib}	-2.4
	HLC	-4.8
$F^{2-} + H^+ \rightarrow FH^-$	$\Delta G_{corr}(H^+)$	-141.8
	$\Delta\Delta G_{Born}$	16.5^a $(27.8)^b$ $(27.0)^c$
	ΔG_{vib}	10.2
	$\Delta G^{(TI-E)}$	-5.7
	$\Delta G^\circ_S(H^+)$	-264.0
	HLC	5.8
$FH^- + H^+ \rightarrow FH_2$	$\Delta G_{corr}(H^+)$	-141.8
	$\Delta\Delta G_{Born}$	5.5^a $(17.7)^b$ $(16.1)^c$
	ΔG_{vib}	8.7
	$\Delta G^{(TI-E)}$	-5.7
	$\Delta G^\circ_S(H^+)$	-264.0
	HLC	-0.3
$FH^\bullet + e^- \rightarrow FH^-$	$\Delta\Delta G_{Born}$	-5.5^a $(-17.7)^a$ $(-16.1)^b$
	ΔG_{vib}	-1.3
	HLC	0.9

[a] Calculated for lumiflavin using eqs 3 and 5. [b] Calculated for MCAD−FAD using eqs 4a and 5. [c] Calculated for CHOX−FAD using eqs 4b and 5.

were -16 kcal/mol (for the reaction $F^{2-} \rightarrow FH^-$) and -23 kcal/mol (for the reaction $FH^- \rightarrow FH_2$). Therefore, the total free-energy change for the two-electron/two-proton reduction of FAD in MCAD was calculated to be -196 kcal/mol (Table 4). This corresponds to a value of -30 mV (Table 5), taking a value of 4.28 V for the standard reduction potential for the NHE[66] and is ~100 mV less negative than two independently reported experimental results on MCAD, which are -137[108] and -135

TABLE 4: Calculated Standard Free Energies of Reaction (kcal/mol) for Electron and Proton Addition Reactions of Lumiflavin, MCAD-Bound FAD, and CHOX-Bound FAD at 298 K

reaction		free-energy changes		
		LF	MCAD−FAD	CHOX−FAD
$F + e^- \rightarrow F^{-\bullet}$	$\Delta G^{(TI-A)}$	−79	−54	−57
	$\Delta G^o(aq)^a$	−93	−81	−82
$F^{-\bullet} + e^- \rightarrow F^{2-}$	$\Delta G^{(TI-A)}$	−94	−41	−35
	$\Delta G^o(aq)^a$	−118	−76	−69
$F^{2-} + H^+ \rightarrow FH^-$	$\Delta G^{(TI-D)}$	144	188	189
	$\Delta G^o(aq)^b$	+17	−16	−18
$FH^- + H^+ \rightarrow FH_2$	$\Delta G^{(TI-D)}$	138	177	175
	$\Delta G^o(aq)^b$	+4	−23	−23
$FH^\bullet + e^- \rightarrow FH^-$	$\Delta G^{(TI-A)}$	−91	−66	−65
	$\Delta G^o(aq)^a$	−97	−84	−82
$F^{-\bullet} + H^+ \rightarrow FH^{\bullet c}$	$\Delta G^o(aq)$	−4	−8	−5
$F + e^- + H^+ \rightarrow FH^\bullet$	$\Delta G^o(aq)$	−97	−89	−87
$F + 2e^- + 2H^+ \rightarrow FH_2$	$\Delta G^o(aq)$	−190	−196	−192

[a] Calculated by eq 13 of section 2.8. [b] Calculated following eq 16 of section 2.9. [c] Calculations used eq 19 of section 3.3.2.

mV.[109] Although the differences between the calculated and experimental standard reduction potentials are 105−107 mV, they correspond to only ∼5.0 kcal/mol when expressed as free-energy differences. Thus, the computed midpoint potential is quite consistent with the experimental results. The pK_a of the N1 proton in the reduced (hydroquinone) state of FAD, calculated using eq 18, was found to be 17 (Table 5).

As noted earlier, the free-energy change of the process $F \rightarrow F^{-\bullet}$ for MCAD is −81 kcal/mol. The free-energy change for a proton addition to $F^{-\bullet}$ contributes an additional −8 kcal/mol (Table 4), and the net free-energy change for $F + e^- + H^+ \rightarrow FH^\bullet$ is −89 kcal/mol (Table 4). The reduction potential $E_{ox,sq}$, predicted from this computation for the oxidized → semiquinone step is −420 mV (taking the standard reduction potential of the NHE as 4.28 V), which may be compared with the experimental value of −155 mV.[108] The pK_a of the N5 proton of the blue semiquinone in MCAD-bound FAD obtained from this computation is 6 (Table 5) and thus quite consistent with the observation[108] of about 20% blue neutral semiquinone in the electrochemical flavin reduction of this enzyme.

3.3.4. CHOX-Bound FAD. Figure 7 shows the variations of $\langle U_f - U_i \rangle_\lambda$ versus λ for various steps, as described in Scheme 4. The free-energy change for the $2e^-/2H^+$ reduction of the CHOX-bound FAD is −192 kcal/mol (Figure 7 and Table 4). The computed value for the midpoint potential, E_m, is −117 mV (Table 5), which has somewhat greater deviations from the experimental value of −278 mV than we found for other

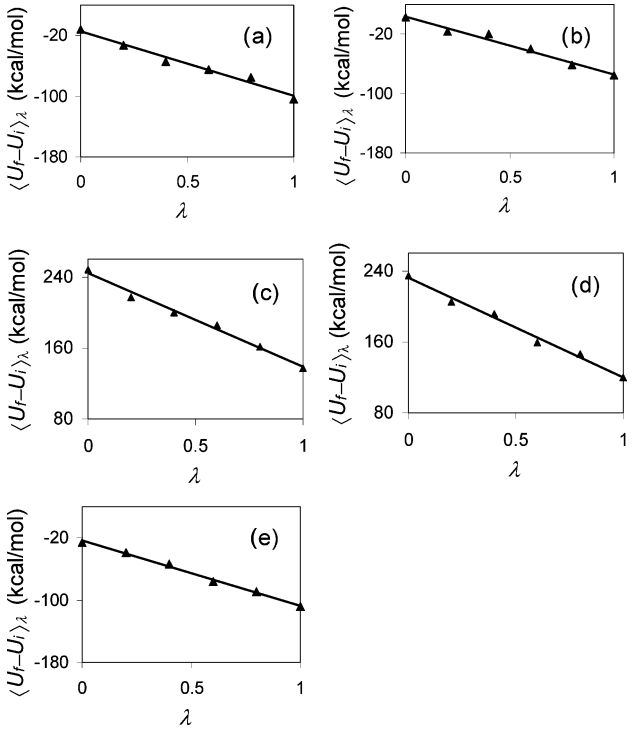

Figure 7. Ensemble-averaged partial derivatives of the potential energy as a function of λ for various reaction steps (shown in Scheme 4) of CHOX-bound FAD.

systems.[110] Recently however, a new value of $E_m = -131$ mV was obtained for CHOX using a different method of measurement.[112] Thus, of the three systems studied, the new E_m value for CHOX shows the best agreement with its calculated value. The first reduction potential $E_{ox,sq}$ (for the $1e^-/1H^+$ process) was obtained as −507 mV, compared with the experimental result of −222 mV.[110] The calculated pK_a of the semiquinone ($FH^\bullet$) in CHOX in this work was 4 (Table 5), which predicts that at neutral pH, the semiquinone in the active site of CHOX will be in its anionic form. The finding is in excellent agreement with the fact that oxidases, unlike the dehydrogenases, stabilize the anionic form of the flavin semiquinone. The pK_a of the semiquinone was ∼4 units lower than that in the free aqueous state; the experimentally known pK_a for the analogous FMN in aqueous solution was 8.55.[7,67] The computed pK_a of the N1 proton of the fully reduced FAD hydroquinone was 17, similar to that observed in MCAD.

Previously, Li et al. reported a reduction potential of −1299 to −1425 mV for $F \rightarrow F^{-\bullet}$ for FAD in CHOX. The first entry in Table 4 gives a computed value of −724 mV (−82 kcal/

TABLE 5: Calculated and Experimental Midpoint Potentials, Calculated Free Energies of Reaction, and pK_a's for Lumiflavin and Enzyme-Bound FADs of MCAD and CHOX at 298 K

reaction	quantity	free-energy changes		
		LF	MCAD−FAD	CHOX−FAD
$F^{-\bullet} + H^+ \rightarrow FH^\bullet$	$\Delta G^o(aq)$ (kcal/mol)	−4	−8	−5
	pK_a	3	6	4
$F + e^- + H^+ \rightarrow FH^\bullet$	$\Delta G^o(aq)$ (kcal/mol)	−97	−89	−87
	calcd $E_{ox,sq}$ (mV)	−74	−420	−507
	exptl $E_{ox,sq}$ (mV)		−155[a]	−222[b]
$FH^- + H^+ \rightarrow LFH_2$	$\Delta G^o(aq)$ (kcal/mol)	+4	−23	−23
	pK_a	−3	17	17
$F + 2e^- + 2H^+ \rightarrow LFH_2$	$\Delta G^o(aq)$ (kcal/mol)	−190	−196	−192
	calcd E_m (mV)	−160	−30	−117
	exptl E_m (mV)	−259[c]	−135[a]	−278[b]

[a] From reference 108. [b] From reference 110. [c] From reference 106.

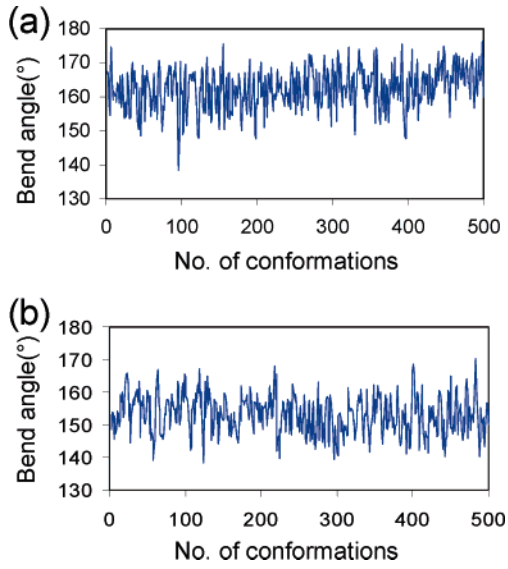

Figure 8. Fluctuations of the flavin bend angle (θ_B, defined as the angle between the planes of the pyrimidine and benzene six-membered rings) with the number of conformations obtained from the trajectory of the MD simulations of (a) MCAD−FAD and (b) MCAD−$FADH_2$.

mol), which is a similar estimate of the one-electron addition process. This is particularly interesting in that although both computations employ the same thermodynamic integration approach to obtain the standard-state free-energy changes in the enzyme, the computational details are quite different. In the work of Li and Cui,[92] molecular dynamics free-energy simulations were carried out using scaled charges on the protein and solvent. This yielded an intermediate free-energy change for the electron addition reaction. Then, a Poisson−Boltzmann continuum electrostatic calculation was made by charging the scaled system to the real values of the standard CHARMM22/TIP3P force field. This procedure was designed to provide good control over the dielectric screening effects in modeling charge annihilation and creation.[113] In the present study, we employed a simple Born correction to account for the long-range electrostatic effects, whereas the simulations were performed employing standard force field parameters. The agreement between these two approaches suggests that free-energy simulations can be performed without the additional step of the charging process in the present system.

3.4. Effect of Enzyme Environment. The bend angle (defined in section 3.1) of the oxidized (neutral) flavin in the aqueous phase is 171°. In contrast, the bend angle (θ_B) of the neutral oxidized flavin in MCAD−FAD, averaged over 500 conformations of equilibrated MD simulations, is 162° (Figure 8a). This demonstrates that the flavin is even more bent than in the reduced hydroquinone state in aqueous solution ($\theta_B = 167°$; see section 3.1) and only 7° less bent than in the fully reduced state in MCAD ($\theta_B = 155°$; Figure 8b). The significant bending of the unreduced flavin in MCAD, illustrated in Figure 9a, is a consequence of strong stereoelectronic interactions of the isoalloxazine ring with four aromatic residues, Tyr133, Trp166, Tyr375, and Phe356, from the second subunit. The flavin ring atoms, the exocyclic oxygen O2, the proton bound to the ring nitrogen N3, and the exocyclic O4 are hydrogen bonded to Val135 (backbone amide proton), Tyr133 (backbone carbonyl), and Thr168 (backbone amide proton), respectively, as shown in Figure 9a.

In CHOX-bound FAD, the flavin ring and its exocyclic substituents interact with three aromatic residues, namely, Tyr107, Tyr446, and Phe487, as shown in Figure 9b. As in

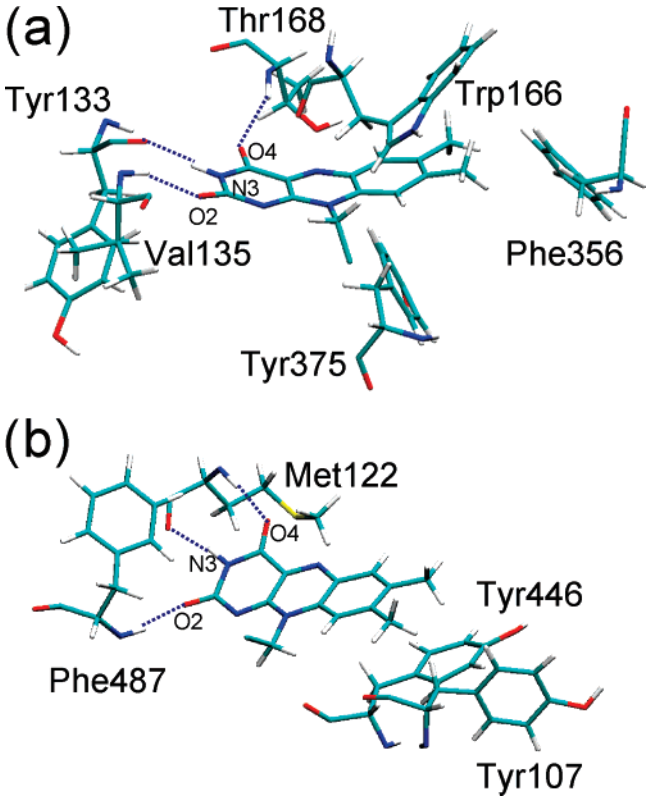

Figure 9. Interacting residues of the flavin binding sites of (a) MCAD and (b) CHOX. The hydrogen bonding interactions are indicated by dotted lines. Color codes for the atoms are the same as those used in Figure 2.

MCAD-bound FAD, the exocyclic O2 atom, the proton bound to N3, and O4 have strong hydrogen-bonding interactions with the backbone amide proton of Phe487, the backbone carbonyl, and amide protons of Met122, respectively, in CHOX. The average bend angle (θ_B) of the oxidized (neutral) flavin in CHOX is 163°, which is similar to the average bend angle observed in the MCAD-bound state.

If the bend angle of flavin is considered to be an indicator of the ease of flavin's reduction,[5] then one would expect that the reduction of flavin in the MCAD-bound flavin would be the most favored one among the three systems, namely, aqueous lumiflavin, CHOX-bound FAD, and MCAD-bound FAD. The present calculations demonstrate that this is true. For MCAD, the free-energy change in the $2e^-/2H^+$ reduction reaction of flavin ($F + 2e^- + 2H^+ \rightarrow FH_2$) is −196 kcal/mol, which is 6 kcal/mol more negative than that for lumiflavin in the aqueous state (Table 5). To verify if the flavin bending is abetting the ease of reduction, we calculated the gas-phase single-point energy of the bent oxidized flavin structure as observed in MCAD. Following a procedure used earlier by Walsh et al.,[5] the bent optimized flavin structure was obtained by constraining two dihedrals, N1−N10−N5−C6 and C9−N10−N5−C4, to 176 and −159°, respectively, as they appear in the MCAD-bound state. The M06-L/6-31+G(d,p) single-point energy of the bent structural form of the oxidized lumiflavin is 5 kcal/mol higher than that in the normal one. The fluctuations of bend angles with conformation number, computed from the stored structures in the trajectory of MCAD−$FADH_2$ MD simulations, are shown in Figure 8b. The computed average (over 500 conformations of the MD simulation) bend angle of the reduced flavin (FH_2) in MCAD is 155° (Figure 8b) and is equal to the gas-phase bend angle of the reduced lumiflavin calculated with B3LYP/6-31+G(d,p), which is 155° (section 3.1). Since the

reduced forms of the aqueous and MCAD-bound structural forms have identical bend angles, the two fully reduced forms are not expected to differ in terms of the energetics. Thus, the destabilization of the oxidized state (5 kcal/mol) alone accounts for the 6 kcal/mol decrease in the total free-energy change of the reduction process as observed in the MCAD-bound flavin.

4. Concluding Notes

Using the SCC-DFTB/CHARMM potential, we have carried out MD simulations of the various reduction steps of flavins in aqueous and enzyme-bound states. The computed midpoint potentials for the $2e^-/2H^+$ reduction of three systems, namely, lumiflavin, MCAD-bound FAD, and CHOX-bound FAD, show reasonable agreement with experimental[106,108,110] results. The computed potentials are −160 mV for lumiflavin, −30 mV for MCAD−FAD, and −117 mV for CHOX−FAD, which are 100, 105, and 161 mV more positive, respectively, than the corresponding experimental[106,109,110] values. (See also ref 112.) The computed $1e^-/1H^+$ reduction potentials agree moderately well with the experimentally determined values[108,110] for these two enzyme systems. The computed potentials are −420 mV for MCAD−FAD and −507 mV for CHOX−FAD. These results are 265 mV (for MCAD−FAD) and 285 mV (for CHOX−FAD) more negative than the experimental data.[108,110] We conclude that the parametrized SCC-DFTB/MM method provides an inexpensive way to predict the midpoint potentials for the $1e^-/1H^+$ and $2e^-/2H^+$ reduction of flavoproteins from their crystal structures.

The calculated pK_a for the N5 proton of lumiflavin semiquinone is 4. The predicted pK_a for the N5 semiquinone proton for cholesterol oxidase is also equal to 4, which is 4 units lower than that for FMN in the aqueous phase.[7,67] This suggests that the anionic semiquinone bound to the active site of the CHOX is stabilized by the enzyme; this result is consistent with the hypothesis[6] of exceptional stabilization of anionic semiquinones by oxidases. The predicted pK_a of the N5 proton of the semiquinone in MCAD-bound FAD is 6, which suggests that the semiquinone is almost neutral at the active site of MCAD. This agrees with the experimental observation[108] of a small amount (20%) of blue (neutral) semiquinone during the electrochemical reduction of MCAD−FAD.

The N1 proton of lumiflavin hydroquinone is predicted by the SCC-DFTB/CHARMM calculations to be highly acidic (pK_a equal to −1.5) and will thus be completely dissociated, which is expected[106] for flavins. However, the computed pK_a's of the two enzyme-bound hydroquinones are quite high, ∼17 for both MCAD and CHOX because the flavin is buried deep into the enzyme pocket with much less solvent accessibility.[114]

The SM6 implicit solvent calculations on aqueous phase enzyme-free lumiflavin differ by less than 1−5 kcal/mol from the results obtained by the explicit solvent SCC-DFTB/MM calculations. This gives added confidence in both treatments. SCC-DFTB predicts accurate bond lengths but is not accurate, when compared to the higher-level DFT calculation, in predicting the equilibrium bend angle after reduction of FAD. Nevertheless, the proton and electron affinities calculated by SCC-DFTB appear to be quite accurate for FAD, and the performance of SCC-DFTB in the reduction potential and pK_a calculations is satisfactory.

The response of an enzyme matrix to a chemical event such as catalysis, oxidation, reduction, or a protonation/deprotonation event involves a combination of geometric, electrostatic, and correlation energy changes in the active site surroundings. The net effect is called reorganization. Reorganization includes electronic polarization and displacement of atomic groups.[107] Therefore, both enzyme reaction rates as well as driving forces are influenced by the geometric and dielectric properties and dispersion-like interaction energies of the active site.[115,116] For a redox-active enzyme, such as MCAD or CHOX, the driving force is directly related to the reduction potential as well as the pK_a of the cofactor and thus is expected to be sensitive to the protein matrix.

It is possible, to some extent, to deconvolute the geometric effects from the electrostatic and dispersion-like effects. For example, in MCAD, it has been observed that the flavin ring geometry is controlled by four hydrophobic residues; this environment results in a significantly bent structure of the enzyme-bound flavin (Figures 8a and 9a), even in the unreduced state. We have explored the contribution of this bent flavin structure (as observed in MCAD) on its reduction potential (section 3.4). We found that bending significantly (∼5 kcal/mol) destabilizes the oxidized state, and thus, the bend angle is a key indicator of the geometric effects of the enzyme matrix on the FAD reduction potential. Other geometric effects such as hydrogen bonding can also be explored by performing suitable mutations[45] on the active site and computing their effects on FAD reduction potentials and pK_a's. The electrostatic contributions of residues can also be quantified by zeroing their charges and computing the free-energy changes.[38] Extending the study to include such calculations might help identify other interactions that are important for determining the reduction potentials and pK_a's of FAD in these enzymes. One question we have not examined is how the enzyme effect on the reduction potential of the cofactor modulates the ability of the cofactor (coenzyme) to serve as an oxidation−reduction catalyst. Since the electron is transferred from the substrate to the flavin in the catalytic process, substrate binding is also expected to have a major influence on these cofactor properties. In order to explore the interconnections between catalysis and the enzyme modulation of the flavin reduction potential, the simulation would have to be extended to a substrate-bound enzyme.

In addition to showing that the SCC-DFTB/MM calculations can predict the free-energy changes of the flavins' various electron- and proton-transfer reactions reasonably accurately for both the free flavin and the two enzyme-bound flavin systems, the present study also has important biological implications resulting from the observations of the role of the enzyme environment. The two charge-transfer steps (the electron addition and the proton addition) of a coupled electron−proton-transfer process can be stepwise or concerted.[1] The first mechanism, but not the second, can involve an intermediate, and conversely, the stabilization of an intermediate favors the first mechanism over the second. The present study implies that a semiquinone intermediate intervenes in the first coupled electron−proton transfer in all of the three flavin systems studied, namely, the free flavin (lumiflavin), the dehydrogenase (MCAD-bound FAD), and the oxidase (CHOX-bound FAD). As observed in this study, the pK_a's of the flavosemiquinones ($F^{-\bullet}$) range from 3 to 6 (Table 5). Thus, the anionic semiquinones are predicted to be stabilized at neutral pH for all three flavin systems, the neutral protonated form being slightly more favored in the dehydrogenase system. The question whether these two charge-transfer processes (electron and proton additions) are concerted or discrete is a question of kinetics and cannot be answered definitively by computing energies of stable and metastable species. However, to the extent that one can draw kinetic inferences from thermodynamic calculations, the stability of the anionic hydroquinone implies that in all the three cases, the

first electron−proton-transfer reaction of flavins occurs through consecutive two-step charge addition processes. In contrast, for the fully reduced hydroquinone state, the N1 proton of the free flavin hydroquinone is acidic, whereas for both enzyme-bound flavins, it is strongly basic (Table 4 and 5). This indicates that in the physiologically relevant pH range, the anionic hydroquinone of the lumiflavin will be stabilized, although both enzymes will stabilize the protonated form. Since the anionic hydroquinone is predicted to be quite unstable at neutral pH, this thermodynamic study suggests that the second coupled electron−proton transfer is more likely to go through a concerted route than a stepwise one.

Acknowledgment. We thank Qiang Cui and Haibo Yu of the University of Wisconsin−Madison and Christopher Cramer, Casey Kelly, Erica Holt, Jingzhi Pu, and Kwangho Nam of the University of Minnesota for helpful discussions. This work was supported in part by the National Institutes of Health, Grant Numbers GM46736 (J.G.) and GM29344 (M.S.), University of Minnesota under Grant Number 1546-519-5976 (M.S.), and by the National Science Foundation under Grant Number CHE03-49122 (D.G.T.). We thank the University of Minnesota Supercomputing Institute for providing resources for computations.

Supporting Information Available: List of all anionic and cationic charged residues and their locations. This material is available free of charge via the Internet at http://pubs.acs.org.

References and Notes

(1) Cukier, R. I. *J. Phys. Chem.* **1996**, *100*, 15428.
(2) Cukier, R. I.; Nocera, D. G. *Annu. Rev. Phys. Chem.* **1998**, *49*, 337.
(3) Ghisla, S.; Massey, V. *Eur. J. Biochem.* **1989**, *181*, 1.
(4) Traber, R.; Kramer, H. E. A.; Hemmerich, P. *Pure Appl. Chem.* **1982**, *54*, 1651.
(5) Walsh, J. D.; Miller, A.-F. *J. Mol. Struct.: THEOCHEM* **2003**, *623*, 185.
(6) Massey, V. *FASEB J.* **1995**, *9*, 473.
(7) Mayhew, S. G. *Eur. J. Biochem.* **1999**, *265*, 698.
(8) Miura, R. *Chem. Rec.* **2001**, *1*, 183.
(9) Warshel, A.; Papayzan, A.; Muegge, I. *J. Biol. Inorg. Chem.* **1997**, *2*, 143.
(10) Reynolds, C. A.; King, P. M.; Richard, W. G. *J. Chem. Soc., Chem. Commun.* **1988**, 1434.
(11) Gunner, M. R.; Honig, B. *Proc. Natl. Acad. Sci. U.S.A.* **1991**, *88*, 9151.
(12) Reynolds, C. A. *Int. J. Quantum Chem.* **1995**, *56*, 677.
(13) Boesch, S. E.; Grafton, A. K.; Wheeler, R. A. *J. Phys. Chem.* **1996**, *100*, 10083.
(14) Raymond, K. S.; Grafton, A. K.; Wheeler, R. A. *J. Phys. Chem. B* **1997**, *101*, 623.
(15) Kettle, L. J.; Bates, S. P.; Mount, A. R. *Phys. Chem. Chem. Phys.* **2000**, *2*, 195.
(16) Winget, P.; Weber, E. J.; Cramer, C. J.; Truhlar, D. G. *Phys. Chem. Chem. Phys.* **2000**, *2*, 1231.
(17) Patterson, E. V.; Cramer, C. J.; Truhlar, D. G. *J. Am. Chem. Soc.* **2001**, *123*, 2025.
(18) Kaszynski, P. *J. Phys. Chem. A* **2001**, *105*, 7626.
(19) Fabre, B.; Hapiot, P.; Simonet, J. *J. Phys. Chem. A* **2002**, *106*, 5422.
(20) Fontanesi, C.; Benassi, R.; Giovanardi, R.; Marcaccio, M.; Paolucci, F.; Roffia, S. *J. Mol. Struct.* **2002**, *612*, 277.
(21) Baik, M. H.; Friesner, R. A. *J. Phys. Chem. A* **2002**, *106*, 7407.
(22) Baik, M. H.; Schauer, C. K.; Ziegler, T. *J. Am. Chem. Soc.* **2002**, *124*, 11167.
(23) Namazian, M.; Norouzi, P.; Ranjbar, R. *J. Mol. Struct.: THEOCHEM* **2003**, *625*, 235.
(24) Winget, P.; Cramer, C. J.; Truhlar, D. G. *Theor. Chem. Acc.* **2004**, *112*, 2025.
(25) Benassi, R.; Ferrarini, P.; Fontanesi, C.; Benedetti, L.; Paolucci, F. *J. Electroanal. Chem.* **2004**, *564*, 231.
(26) Namazian, M.; Almodarresieh, H. A. *J. Mol. Struct.: THEOCHEM* **2004**, *686*, 97.
(27) Fu, Y.; Liu, L.; Yu, H. Z.; Wang, Y. M.; Guo, Q. X. *J. Am. Chem. Soc.* **2005**, *127*, 7227.
(28) Dutton, A. S.; Fukuto, J. M.; Houk, K. N. *Inorg. Chem.* **2005**, *44*, 4024.
(29) Camurri, G.; Ferrarini, P.; Giovanardi, R.; Fontanesi, R. B. C. *J. Electroanal. Chem.* **2005**, *585*, 181.
(30) Shamshipur, M.; Alizadeh, K.; Arshadi, S. *J. Mol. Struct.: THEOCHEM* **2006**, *758*, 71.
(31) Wass, J.; Ahlberg, E.; Panas, I.; Schiffrin, D. J. *J. Mol. Struct.: THEOCHEM* **2006**, *758*, 2005.
(32) Bottoni, A.; Cosimelli, B.; Scavetta, E.; Spinelli, D.; Spisani, R.; Stenta, M.; Tonelli, D. *Mol. Phys.* **2006**, *104*, 2961.
(33) Jaque, P.; Marenich, A. V.; Cramer, C. J.; Truhlar, D. G. *J. Phys. Chem. C* **2007**, *111*, 5783.
(34) Tsushima, S.; Wahlgren, U.; Grenthe, I. *J. Phys. Chem. A* **2006**, *110*, 9175.
(35) Churg, A. K.; Warshel, A. *Biochemistry* **1986**, *25*, 1675.
(36) Shenoy, V. S.; Ichiye, T. *Proteins* **1993**, *17*, 152.
(37) Ichiye, T. In *Computational Biochemistry and Biophysics*; Becker, O. M., MacKerell, A. D. J., Roux, B., Watanabe, M., Eds.; Dekker: New York, 2001; pp 393.
(38) Formaneck, M. S.; Li, G.; Xiaodong, Z.; Cui, Q. *J. Theor. Comput. Chem.* **2002**, *1*, 53.
(39) Tavernelli, I.; Vuilleurmier, R.; Sprik, M. *Phys. Rev. Lett.* **2002**, *88*, 213002.
(40) Li, G.; Zhang, X.; Cui, Q. *J. Phys. Chem. B* **2003**, *107*, 8643.
(41) Olsson, M. H.; Hong, G.; Warshel, A. *J. Am. Chem. Soc.* **2003**, *125*, 5025.
(42) Li, H.; Webb, S. P.; Ivanic, J.; Jensen, J. H. *J. Am. Chem. Soc.* **2004**, *126*, 8010.
(43) Blumberger, J.; Sprik, M. *Theor. Chem. Acc.* **2006**, *115*, 113.
(44) Poulsen, T. D.; Garcia-Viloca, M.; Gao, J.; Truhlar, D. G. *J. Phys. Chem. B* **2003**, *107*, 9567.
(45) Bhattacharyya, S.; Ma, S.; Stankovich, M. T.; Truhlar, D. G.; Gao, J. *Biochemistry* **2005**, *44*, 16549.
(46) Dewar, M. J. S.; Zoebisch, E. G.; Healy, E. F.; Stewart, J. J. P. *J. Am. Chem. Soc.* **1985**, *107*, 3902.
(47) MacKerell, A. D. J.; Bashford, D.; Bellott, M.; Dunbrack, R. L. J.; Evanseck, J. D.; Field, M. J.; Fischer, S.; Gao, J.; Gou, J.; Ha, S.; Joseph-McCarthy, D.; Kuchnir, L.; Kuczera, K.; Lau, F. T. K.; Mattos, C.; Michnick, S.; Ngo, T.; Nguyen, D. T.; Prodhom, B.; Reiher, W. E. I.; Roux, B.; Schelenkrich, M.; Smith, J. C.; Stote, R.; Straub, J.; Watanbe, M.; Wiórkiewicz-Kuczera, J.; Yin, D.; Karplus, M. *J. Phys. Chem. B* **1998**, *102*, 3586.
(48) Elstner, M.; Porezag, D.; Jungnickel, G.; Elstner, J.; Haugk, M.; Frauenheim, T.; Suhai, S.; Seifert, G. *Phys. Rev. B* **1998**, *58*, 7260.
(49) Frauenheim, T.; Seifert, G.; Elstner, M.; Hajnal, Z.; Jungnickel, G.; Porezag, D.; Suhai, S.; Rcholz, R. *Phys. Status Solidi B* **2000**, *217*, 41.
(50) Cui, Q.; Elstner, M.; Kaxiras, E.; Frauenheim, T.; Karplus, M. *J. Phys. Chem. B* **2001**, *105*, 569.
(51) Zhao, Y.; Truhlar, D. G. *J. Chem. Phys.* **2006**, *125*, 194101.
(52) Becke, A. D. *Phys. Rev. A* **1988**, *38*, 3098.
(53) Lee, C.; Yang, W.; Parr, R. G. *Phys. Rev. B* **1988**, *37*, 785.
(54) Stephens, P. J.; Devlin, F. J.; Chabalowski, C. F.; Frisch, M. J. *J. Phys. Chem.* **1994**, *98*, 11623.
(55) Hariharan, P. C.; Pople, J. A. *Theor. Chim. Acta* **1973**, *28*, 213.
(56) Zerner, M. C. *Rev. Comput. Chem.* **1991**, *8*, 313.
(57) Slater, J. C.; Koster, G. F. *Phys. Rev.* **1954**, *94*, 1498.
(58) Elstner, M.; Cui, Q.; Munih, P.; Kaxiras, E.; Frauenheim, T.; Karplus, M. *J. Comput. Chem.* **2003**, *24*, 565.
(59) Perdew, J. P.; Burke, K.; Ernzerhof, M. *Phys. Rev. Lett.* **1996**, *77*, 3865.
(60) Kelly, C. P.; Cramer, C. J.; Truhlar, D. G. *J. Chem. Theory Comput.* **2005**, *1*, 1133.
(61) Kelly, C. P.; Cramer, C. J.; Truhlar, D. G. *J. Phys. Chem. A* **2006**, *110*, 2493.
(62) Bartnmess, J. E. *J. Phys. Chem.* **1994**, *98*, 6420.
(63) Frisch, M. J.; Trucks, G. W.; Schlegel, H. B.; Scuseria, G. E.; Robb, M. A.; Cheeseman, J. R.; Montgomery, J. A., Jr.; Vreven, T.; Kudin, K. N.; Burant, J. C.; Millam, J. M.; Iyengar, S. S.; Tomasi, J.; Barone, V.; Mennucci, B.; Cossi, M.; Scalmani, G.; Rega, N.; Petersson, G. A.; Nakatsuji, H.; Hada, M.; Ehara, M.; Toyota, K.; Fukuda, R.; Hasegawa, J.; Ishida, M.; Nakajima, T.; Honda, Y.; Kitao, O.; Nakai, H.; Klene, M.; Li, X.; Knox, J. E.; Hratchian, H. P.; Cross, J. B.; Bakken, V.; Adamo, C.; Jaramillo, J.; Gomperts, R.; Stratmann, R. E.; Yazyev, O.; Austin, A. J.; Cammi, R.; Pomelli, C.; Ochterski, J. W.; Ayala, P. Y.; Morokuma, K.; Voth, G. A.; Salvador, P.; Dannenberg, J. J.; Zakrzewski, V. G.; Dapprich, S.; Daniels, A. D.; Strain, M. C.; Farkas, O.; Malick, D. K.; Rabuck, A. D.; Raghavachari, K.; Foresman, J. B.; Ortiz, J. V.; Cui, Q.; Baboul, A. G.; Clifford, S.; Cioslowski, J.; Stefanov, B. B.; Liu, G.; Liashenko, A.; Piskorz, P.; Komaromi, I.; Martin, R. L.; Fox, D. J.; Keith, T.; Al-Laham, M. A.; Peng, C. Y.; Nanayakkara, A.; Challacombe, M.; Gill, P. M. W.; Johnson, B.; Chen, W.; Wong, M. W.; Gonzalez, C.; Pople, J. A. *Gaussian 03*, revision C.02; Gaussian, Inc.: Wallingford, CT, 2004.

(64) Chamberlin, A. C.; Kelly, C. P.; Thompson, J. D.; Xidos, J. D.; Li, J.; Hawkins, G. D.; Winget, P. D.; Zhu, T.; Rinaldi, D.; Liotard, D. A.; Cramer, C. J.; Truhlar, D. G.; Frisch, M. J. *MN-GSM*, version 6.0; University of Minnesota: Minneapolis, MN 55455-0431, 2005.

(65) Lewis, A.; Bumpus, J. A.; Truhlar, D. G.; Cramer, C. J. *J. Chem. Educ.* **2004**, *81*, 596.

(66) Kelly, C. P.; Cramer, C. J.; Truhlar, D. G. *J. Phys. Chem. B* **2006**, *110*, 16066.

(67) Draper, R. D.; Ingraham, L. L. *Arch. Biochem. Biophys.* **1968**, *125*, 802.

(68) Mancini-Samuelson, G. J.; Kieweg, V.; Sabaj, K. M.; Ghisla, S.; Stankovich, M. T. *Biochemistry* **1998**, *37*, 14605.

(69) Brooks, C. L., III; Brunger, A.; Karplus, M. *Biopolymers* **1985**, *24*, 843.

(70) Brooks, C. L. I.; Karplus, M. *J. Chem. Phys.* **1983**, *79*, 6312.

(71) Kim, J. J.; Wang, M.; Paschke, R. *Proc. Natl. Acad. Sci. U.S.A.* **1993**, *90*, 7523.

(72) Yue, Q. K.; Kass, I. J.; Sampson, N. S.; Vrielink, A. *Biochemistry* **1999**, *38*, 4277.

(73) Berman, H. M.; Westbrook, J.; Feng, Z.; Gilliland, G.; Bhat, T. N.; Weissig, H.; Shindyalov, I. N.; Bourne, P. E. *Nucleic Acids Res.* **2000**, *28*, 235.

(74) Brooks, B. R.; Bruccoleri, R. E.; Olafson, B. D.; States, D. J.; Swaminathan, S. J. *J. Comput. Chem.* **1983**, *4*, 187.

(75) Born, M. *Z. Phys.* **1920**, *1*, 45.

(76) Cramer, C. J.; Truhlar, D. G. *Chem. Rev.* **1999**, *99*, 2161.

(77) Pavelites, J. J.; Gao, J. L.; Bash, P. A.; MacKerell, A. D., Jr. *J. Comput. Chem.* **1997**, *18*, 221.

(78) MacKerell, A. D., Jr.; Bashford, D.; Bellott, M.; Dunbrack, R. L., Jr.; Evanseck, J. D.; Field, M. J.; Fischer, S.; Gao, J.; Gou, J.; Ha, S.; Joseph-McCarthy, D.; Kuchnir, L.; Kuczera, K.; Lau, F. T. K.; Mattos, C.; Michnick, S.; Ngo, T.; Nguyen, D. T.; Prodhom, B.; Reiher, W. E., III; Roux, B.; Schelenkrich, M.; Smith, J. C.; Stote, R.; Straub, J.; Watanbe, M.; Wiórkiewicz-Kuczera, J.; Yin, D.; Karplus, M. *J. Phys. Chem. B* **1998**, *102*, 3586.

(79) Jorgensen, W. L.; Chandrasekhar, J.; Madura, J. D.; Impey, R. W.; Klein, M. L. *J. Chem. Phys.* **1983**, *79*, 926.

(80) Rychaert, J. P.; Ciotti, G.; Berensden, H. J. C. *J. Comput. Phys.* **1977**, *23*, 327.

(81) Verlet, L. *Phys. Rev.* **1967**, *159*, 98.

(82) Hockney, R. W. *Methods Comput. Phys.* **1970**, *9*, 136.

(83) Gao, J.; Amara, P.; Alhambra, C.; Field, M. *J. Phys. Chem. A* **1998**, *102*, 4714.

(84) Amara, P.; Field, M.; Alhambra, C.; Gao, J. *Theor. Chem. Acc.* **2000**, *104*, 336.

(85) Field, M. J.; Bash, P. A.; Karplus, M. *J. Comput. Chem.* **1990**, *11*, 700.

(86) Beveridge, D. L.; Mezei, M.; Ravishanker, G.; Jayaram, B. *J. Biosci.* **1985**, *8*, 167.

(87) Mezei, M.; Beveridge, D. L. *Ann. N.Y. Acad. Sci.* **1986**, *482*, 1.

(88) Straatsma, T. P.; Berensden, H. J. C. *J. Chem. Phys.* **1988**, *89*, 5876.

(89) Gao, J.; Kucezera, K.; Tidor, B.; Karplus, M. *Science* **1989**, *244*, 1069.

(90) Simonson, T. In *Computational Biochemistry and Biophysics*; Becker, O. M., MacKerell, A. D., Jr., Roux, B., Watanabe, M., Eds.; Dekker: New York, 2001; pp 169.

(91) Frenkel, D.; Smit, B. *Understanding Molecular Simulation*; Academics: San Deigo, CA, 2002; pp 168ff.

(92) Li, G.; Cui, Q. *J. Phys. Chem. B* **2003**, *107*, 14521.

(93) Gao, J.; Xia, X. *Science* **1992**, *258*, 631.

(94) Tissandier, M. D.; Cowen, K. A.; Feng, W. Y.; Gundlach, E.; Cohen, M. H.; Earhart, A. D.; Coe, J. V.; Tuttle, T. R., Jr. *J. Phys. Chem. A* **1998**, *102*, 7787.

(95) Camaioni, D. M.; Schwerdtfeger, C. A. *J. Phys. Chem. A* **2005**, *109*, 10795.

(96) Riccardi, D.; Schaefer, P.; Cui, Q. *J. Phys. Chem. B* **2005**, *109*, 17715.

(97) Herschbach, D. R.; Johnston, H. S.; Rapp, D. *J. Chem. Phys.* **1959**, *31*, 1652.

(98) Boresche, T. *Mol. Simul.* **2002**, *28*, 13.

(99) Xie, L.; Liu, H. *J. Comput. Chem.* **2002**, *23*, 1404.

(100) Smedarchina, Z.; Siebrand, W.; Fernandez-Ramos, A.; Cui, Q. *J. Am. Chem. Soc.* **2003**, *125*, 243.

(101) Kumar, A.; Knapp-Mohammady, M.; Mishra, P. C.; Suhai, S. *J. Comput. Chem.* **2004**, *25*, 1047.

(102) Witek, H. A.; Morokuma, K. *J. Comput. Chem.* **2004**, *25*, 1858.

(103) Witek, H. A.; Morokuma, K.; Stradomska, A. *J. Chem. Phys.* **2004**, *121*, 5171.

(104) Macheroux, P.; Ghisla, S.; Sanner, C.; Ruterjans, H.; Muller, F. *BMC Biochem.* **2005**, *6*, 26.

(105) Lowe, H. J.; Clark, W. M. *J. Biol. Chem.* **1956**, *221*, 983.

(106) Hasford, J. J.; Rizzo, C. J. *J. Am. Chem. Soc.* **1998**, *120*, 2251.

(107) Simonson, T. *Proc. Natl. Acad. Sci. U.S.A.* **2002**, *99*, 6544.

(108) Gustafson, W. G.; Feinberg, B. A.; McFarland, J. T. *J. Biol. Chem.* **1986**, *261*, 7733.

(109) Lenn, N. D.; Stankovich, M. T.; Liu, H. W. *Biochemistry* **1990**, *29*, 3709.

(110) Yin, Y.; Sampson, N. S.; Vrielink, A.; Lario, P. I. *Biochemistry* **2001**, *40*, 13779.

(111) Venkataram, U. V.; Bruice, T. C. *J. Am. Chem. Soc.* **1984**, *106*, 5703.

(112) Sampson, N. S.; Chen, L. Personal communication.

(113) Simonson, T.; Archontis, G.; Karplus, M. *J. Phys. Chem. B* **1997**, *101*, 8349.

(114) Fleischmann, G.; Lederer, F.; Muller, F.; Bacher, A.; Ruterjans, H. *Eur. J. Biochem.* **2000**, *267*, 5156.

(115) Marcus, R. A.; Sutin, N. *Biochim. Biophys. Acta* **1985**, *811*, 265.

(116) Warshel, A.; Aqvist, J. *Annu. Rev. Biophys. Biophys. Chem.* **1991**, *20*, 267.

(117) Range, K.; Riccardi, D.; Cui, Q.; Elstner, M.; York, D. M. *Phys. Chem. Chem. Phys.* **2005**, *7*, 3070.